

H₂O₂ enhanced Ca²⁺ currents through P/Q-type Ca²⁺ channels composed of α 1A, α 2 δ , and β 3 subunits at potentials more negative than 0 mV [9]. The discrepancy may be due to differences in experimental conditions. For example, we examined the Ca²⁺ current of cultured dentate granule cells, whereas the previous study measured the current permeating through cloned neuronal Ca²⁺ channels expressed in *Xenopus* oocytes.

The exact mechanisms whereby H₂O₂ selectively enhances the nifedipine-sensitive Ca²⁺ current still remain to be elucidated. Pretreatment with the ER stressor tunicamycin did not affect the Ca²⁺ current. Taken together, these results suggest that oxidative stress may selectively regulate the activity of L-type Ca²⁺ channels in dentate granule cells. Currents through VGCCs are known to be increased by phosphorylation of channel α subunit proteins [18]. H₂O₂ may directly or indirectly increase phosphorylation of the α subunit of L-type Ca²⁺ channels.

Acknowledgements

This work was partly supported by Health and Labour Science Research Grants for Research on Advanced Medical Technology from the Ministry of Health, Labour and Welfare, Japan and a grant-in-aid for scientific research from the Ministry of Education, Culture, Sports, Science, and Technology, Japan (KAKENHI13672319) awarded to K.K.

References

- [1] L.S. Eliot, D. Johnston, Multiple components of calcium current in acutely dissociated dentate gyrus granule neurons, *J. Neurophysiol.* 72 (1994) 762–777.
- [2] Y. Ikegaya, N. Nishiyama, N. Matsuki, L-Type Ca²⁺ channel blocker inhibits mossy fiber sprouting and cognitive deficits following pilocarpine seizures in immature mice, *Neuroscience* 98 (2000) 647–659.
- [3] K. Ishige, Q. Chen, Y. Sagara, D. Schubert, The activation of dopamine D4 receptors inhibits oxidative stress-induced nerve cell death, *J. Neurosci.* 21 (2001) 6069–6076.
- [4] K. Ishige, D. Schubert, Y. Sagara, Flavonoids protect neuronal cells from oxidative stress by three distinct mechanisms, *Free Radic. Biol. Med.* 30 (2001) 433–446.
- [5] K. Ito, K. Nakazawa, S. Koizumi, M. Liu, K. Takeuchi, T. Hashimoto, Y. Ohno, K. Inoue, Inhibition by antipsychotic drugs of L-type Ca²⁺ channel current in PC12 cells, *Eur. J. Pharmacol.* 314 (1996) 143–150.
- [6] Y. Ito, M. Arakawa, K. Ishige, H. Fukuda, Comparative study of survival signal withdrawal and hydroxymenonol-induced cell death in cerebellar granule cells, *Neurosci. Res.* 35 (1999) 321–327.
- [7] Y. Ito, Y. Kosuge, T. Sakikubo, K. Horie, N. Ishikawa, N. Obokata, E. Yokoyama, K. Yamashina, M. Yamamoto, H. Saito, M. Arakawa, K. Ishige, Protective effect of S-allyl-L-cysteine, a garlic compound, on amyloid β -protein-induced cell death in nerve growth factor-differentiated PC12 cells, *Neurosci. Res.* 46 (2003) 119–125.
- [8] Y. Kosuge, Y. Koen, K. Ishige, K. Minami, H. Urasawa, H. Saito, Y. Ito, S-Allyl-L-cysteine selectively protects cultured rat hippocampal neurons from amyloid β -protein- and tunicamycin-induced neuronal death, *Neuroscience* (2004) in press.
- [9] A. Li, J. Segui, S.H. Heinemann, T. Hoshi, Oxidation regulates cloned neuronal voltage-dependent Ca²⁺ channels expressed in *Xenopus* oocytes, *J. Neurosci.* 18 (1998) 6740–6747.
- [10] R.J. Mark, M.A. Lovell, W.R. Markesbery, K. Uchida, M.P. Mattson, A role for 4-hydroxynonenal, an aldehydic product of lipid peroxidation, in disruption of ion homeostasis and neuronal death induced by amyloid β -peptide, *J. Neurochem.* 68 (1997) 255–264.
- [11] G.P. Miljanich, J. Ramachandran, Antagonists of neuronal calcium channels: structure, function, and therapeutic implications, *Annu. Rev. Pharmacol. Toxicol.* 35 (1995) 707–734.
- [12] W. Müller, K. Bittner, Differential oxidative modulation of voltage-dependent K⁺ currents in rat hippocampal neurons, *J. Neurophysiol.* 87 (2002) 2990–2995.
- [13] W.A. Pedersen, W. Fu, J.N. Keller, W.R. Markesbery, S. Appel, R.G. Smith, E. Kasarskis, M.P. Mattson, Protein modification by the lipid peroxidation product 4-hydroxynonenal in the spinal cords of amyotrophic lateral sclerosis patients, *Ann. Neurol.* 44 (1998) 819–824.
- [14] Y. Sagara, K. Ishige, C. Tsai, P. Maher, Tyrphostins protect neuronal cells from oxidative stress, *J. Biol. Chem.* 277 (2002) 36204–36215.
- [15] R. Sah, F. Galeffi, R. Ahrens, G. Jordan, R.D. Schwartz-Bloom, Modulation of the GABA_A-gated chloride channel by reactive oxygen species, *J. Neurochem.* 80 (2002) 383–391.
- [16] B.A. Yankner, Mechanisms of neuronal degeneration in Alzheimer's disease, *Neuron* 16 (1996) 921–932.
- [17] A. Yoritaka, N. Hattori, K. Uchida, M. Tanaka, E.R. Stadtman, Y. Mizuno, Immunohistochemical detection of 4-hydroxynonenal protein adducts in Parkinson disease, *Proc. Natl. Acad. Sci. USA* 93 (1996) 2696–2701.
- [18] G.W. Zamponi, E. Bourinet, D. Nelson, J. Nargeot, T.P. Snutch, Crosstalk between G proteins and protein kinase C mediated by the calcium channel α 1 subunit, *Nature* 385 (1997) 442–446.

Available online at www.sciencedirect.com

SCIENCE @ DIRECT®

European Journal of Pharmacology xx (2004) xxx–xxx

EJP

www.elsevier.com/locate/ejphar

1

2 Characterization of voltage-dependent gating of P2X₂ receptor/channel

3 Ken Nakazawa*, Yasuo Ohno

4 Cellular and Molecular Pharmacology Section, Division of Pharmacology, National Institute of Health Sciences, 1-18-1 Kamiyoga, Setagaya,
5 Tokyo 158-8501, Japan

6 Received 9 September 2004; received in revised form 29 November 2004; accepted 6 December 2004

7

8 Abstract

9 The role of a voltage-dependent gate of recombinant P2X₂ receptor/channel was investigated in *Xenopus* oocytes. When a voltage step to
10 –110 mV was applied from a holding potential of –50 mV, a gradual increase was observed in current evoked by 30 μM ATP. Contribution
11 of this voltage-dependent component to total ATP-evoked current was greater when the current was evoked by lower concentrations of ATP.
12 The voltage-dependent gate closed upon depolarization, and half the gates were closed at –80 mV. On the other hand, a potential at which
13 half the gates opened was about –30 mV or more positive, which was determined using a series of hyperpolarization steps. The results of the
14 present study suggest that the voltage-dependent gate behavior of P2X₂ receptor is not due to simple activation and deactivation of a single
15 gate, but rather due to transition from a low to a high ATP affinity state.
16 © 2004 Published by Elsevier B.V.

17 **Keywords:** P2X receptor; Voltage dependence; Gate; Kinetics; Ligand affinity18
19 1. Introduction

20 Extracellular ATP is considered a neurotransmitter, and its
21 fast neurotransmission is mediated through ion channel-
22 forming P2X receptors (see reviews, Ralevic and Burnstock,
23 1998; Khakh, 2001; North, 2002). To date, at least seven
24 subclasses of P2X receptor (P2X_{1–7}) have been cloned, which
25 form homo- or heteromeric receptors that act as functional ion
26 channels (North and Surprenant, 2000). Each subclass
27 consists of two transmembrane domains (TM1 and TM2)
28 and one long extracellular domain (E1) between them. Both
29 TM1 (Jiang et al., 2001; Haines et al., 2001) and TM2
30 (Rassendren et al., 1997; Egan et al., 1998; Migita et al.,
31 2001) contribute to formation of the channel pore. P2X
32 receptor/channels are permeable to cations, but demonstrate
33 poor cation selectivity. The channels are gated by ATP
34 molecules, and the narrowest part of the channel pore opens
35 when activated (Rassendren et al., 1997). The ATP-binding
36 site for gating is partly attributable to basic amino acid
37 residues near the outer mouth of the channel pore formed by

TM1 and TM2 (Ennion et al., 2000; Jiang et al., 2000), and 38
the possibility that aromatic residues in E1 contribute to the 39
binding site has also been suggested (Nakazawa et al., 2002; 40
Roberts and Evans, 2004). 41

In addition to ATP, other factors are known to modulate 42
channel activity. Zn²⁺ and acidic conditions facilitate ATP- 43
mediated gating by increasing ATP sensitivity of P2X₂ 44
receptor (Clyne et al., 2002). Neurotransmitters, including 45
dopamine, and related compounds also facilitate ATP- 46
mediated gating (Nakazawa et al., 1997a). Membrane 47
potential may also play a role. It has been reported that 48
ionic current activated by ATP is enhanced by hyper- 49
polarization in pheochromocytoma PC12 cells (Nakazawa et 50
al., 1997b). We observed similar voltage-dependent gating 51
of recombinant P2X₂ receptor/channel, which was origi- 52
nally cloned from PC12 cells (Brake et al., 1994), and 53
qualitatively analyzed its properties in the present study. 54

2. Methods 55

Recordings of ionic current through recombinant P2X₂ 56
receptor/channels were performed according to our previous 57

* Corresponding author. Tel.: +81 3 3700 9704; fax: +81 3 3707 6950.
E-mail address: nakazawa@nihs.go.jp (K. Nakazawa).

58 report (Nakazawa and Ohno, 1997). Briefly, the cloned rat
 59 P2X₂ receptor (Brake et al., 1994) was expressed in
 60 *Xenopus* oocytes by injecting in vitro transcribed cRNA.
 61 After 4 days of incubation at 18 °C, the membrane current
 62 of the oocytes was recorded. Oocytes were bathed in ND96
 63 solution containing (in mM) NaCl 96, KCl 2, CaCl₂ 1.8,
 64 MgCl₂ 1, HEPES 5 (pH 7.5 with NaOH). In some
 65 experiments, oocytes were bathed in solution containing
 66 10.8 mM BaCl₂ instead of 1.8 mM CaCl₂. When achieving
 67 a low extracellular chloride concentration, 96 mM Na-
 68 acetate was added instead of 96 mM NaCl. ATP (adenosine
 69 5'-triphosphate disodium salt; Sigma, St. Louis, MO,
 70 U.S.A.) was applied by superfusion for approximately 10
 71 s at regular 2-min intervals. Membrane current was
 72 recorded using the standard two-electrode voltage-clamp
 73 techniques, and electrical signals were stored on a data
 74 recorder (PC204Ax; SONY, Tokyo, Japan) for off-line
 75 analysis. Curve fittings to data were made using Microsoft'
 76 Excel X.

77 3. Results

78 3.1. Voltage-dependent component of ATP-evoked current

79 Fig. 1A compares membrane currents in the absence and
 80 presence of 30 μM ATP in a P2X₂ receptor-expressing
 81 oocyte. The oocyte was held at -50 mV and stepped to
 82 -110 mV for 200 ms. In the presence of ATP, inward
 83 current at -110 mV did not instantaneously reach steady-
 84 state, but gradually increased: a biphasic increase in current
 85 was observed with a voltage-independent component ("a" in
 86 Fig. 1A) and a voltage-dependent component ("b" in Fig.
 87 1A). When the voltage was returned to -50 mV, a gradually
 88 declining inward "tail" current was observed ("c" in Fig.
 89 1A). The voltage-dependent component of the inward
 90 current at -110 mV was observed to follow first-order
 91 kinetics with a time constant of 40 ms (Fig. 1B).

92 Fig. 2A demonstrates an increased magnitude of the
 93 voltage-dependent component when activated from a less
 94 negative holding potential. The voltage-dependent compo-
 95 nent was larger when the step to -110 mV was applied from
 96 -10 mV ("a" in Fig. 2A) than when it was applied from
 97 -70 mV ("b" in Fig. 2A). This dependence of the voltage-
 98 dependent component on holding potentials is illustrated in
 99 Fig. 2B. It is worth noting that Ca²⁺-activated currents exist
 100 in *Xenopus* oocytes (Weber, 1999; Zhang and Hamill,
 101 2000). Since P2X receptor/channels are Ca²⁺-permeable
 102 (Khakh, 2001), a secondarily activated Ca²⁺-induced current
 103 might contribute to the observed voltage-dependent
 104 changes. This does not, however, appear to be the case
 105 since a similar dependence on holding potentials was
 106 observed when extracellular Ca²⁺ was replaced with 10.8
 107 mM Ba²⁺. Time constants for the activation of the voltage-
 108 dependent component were obtained as shown in Fig. 1B,
 109 and the mean values were plotted against holding potentials

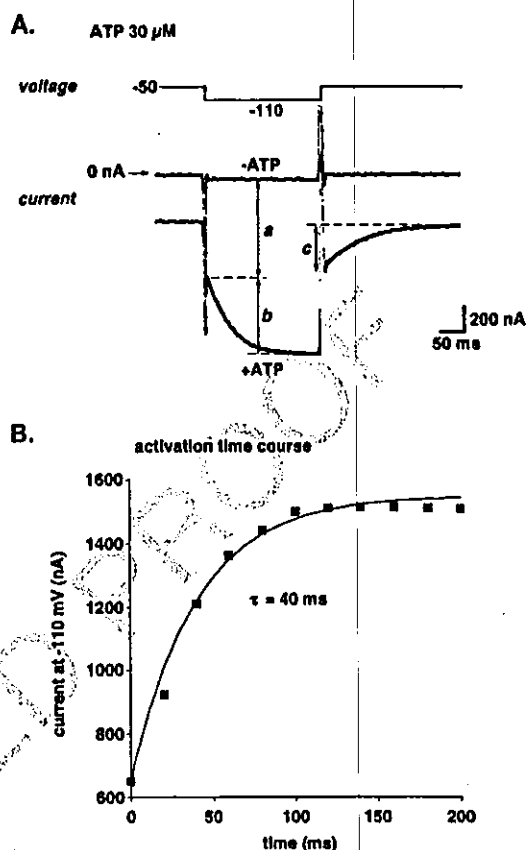


Fig. 1. (A) Current traces of an oocyte stepped to -110 mV from a holding potential of -50 mV in the absence (-ATP) or presence (+ATP) of 30 μM ATP. The current evoked by ATP is represented by the difference between the two traces. Upon hyperpolarization, a gradual increase in current was observed in the presence of ATP, suggesting activation of a voltage-dependent gate (denoted by "b"). The current denoted by "c" represents a gradually declining "tail current" that was observed when the voltage was returned to -50 mV. (B) Time course of activation of the voltage-dependent component. Current amplitude of the voltage-dependent component represented by "b" in panel A was plotted against time after the onset of hyperpolarization at -110 mV. The voltage-dependent component could be made to fit a curve with a time constant of 40 ms.

(Fig. 2C). While the current amplitude demonstrated voltage dependence (Fig. 2B), voltage did not have an effect on time course of the activation. 110
111
112

3.2. Effect of ATP concentrations 113

Fig. 3A shows the voltage-dependent component of the current activated by 10 μM or 300 μM of ATP in a single oocyte. The relative size of the voltage-dependent component involved in total ATP-evoked current became smaller when the current was evoked by greater concentrations of ATP (Fig. 3A and B). A similar dependence on ATP concentration was observed for the current evoked in the presence of 10.8 mM Ba²⁺ instead of 1.8 mM Ca²⁺ (Fig. 3B). Dependence on ATP concentrations was also found for activation time constants for the voltage- 114
115
116
117
118
119
120
121
122
123

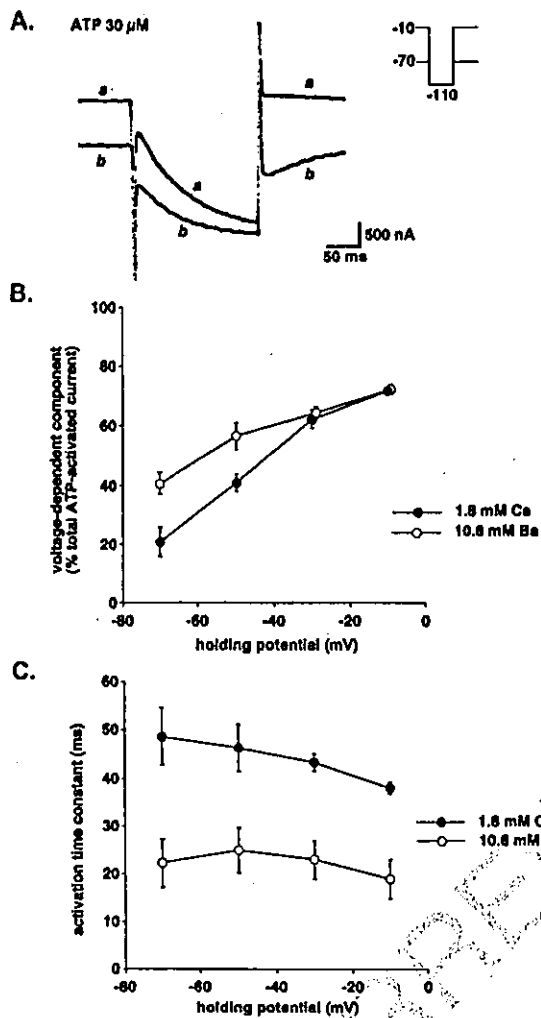


Fig. 2. Effect of holding potential on current. Current was evoked by 30 μM ATP. (A) Voltage-dependent current at -110 mV when stepped from a holding potential of -10 mV ("a") or -70 mV ("b"). (B) Effect of holding potential on voltage-dependent current. The amplitude of the voltage-dependent current was measured as described in Fig. 1A. Mean values obtained from 4 oocytes in a standard extracellular solution containing 1.8 mM Ca^{2+} (\bullet) and an extracellular solution containing 10.8 mM Ba^{2+} (instead of Ca^{2+} ; \circ) were plotted. Bars represent the S.E.M. (C) Time course of activation of the voltage-dependent component. Time constants were determined as shown in Fig. 1B, and mean values obtained from 4 oocytes were plotted against holding potentials. Bars represent the S.E.M.

124 dependent component; the time constants were larger for
125 10 μM ATP than 30 μM ATP (Fig. 3C).

126 3.3. Activation and deactivation kinetics

127 Cl^- currents are observed in *Xenopus* oocytes (Weber,
128 1999; Zhang and Hamill, 2000). In the following experi-
129 ments, current measurements were made using an
130 extracellular solution containing 96 mM Na-aspartate
131 instead of NaCl in order to facilitate the analysis of the

voltage-dependent component of ATP-evoked current by
132 reducing Cl^- currents. In doing so, there was an obvious
133 reduction in outward current upon depolarization, result-
134 ing in better voltage-clamp conditions. Using this
135 extracellular solution, the EC_{50} value for ATP-activated
136 current measured at -50 mV was about 40 μM , which
137 was lower than the value obtained with the standard
138 extracellular solution containing 96 mM NaCl (about
139 100 μM ; Nakazawa and Ohno, 2004). Fig. 4 illustrates
140

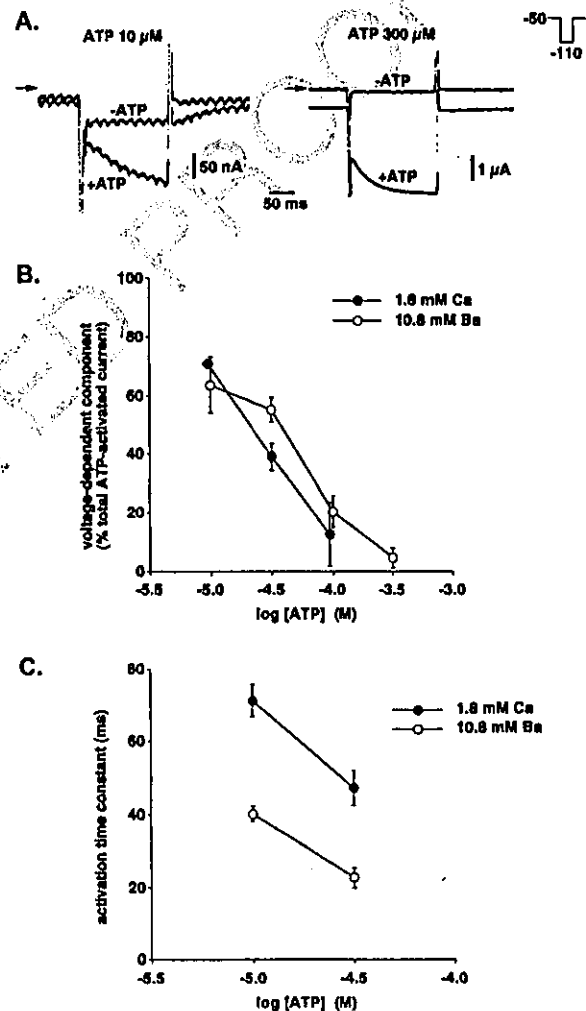


Fig. 3. Effect of ATP concentration. The voltage-dependent current was activated by hyperpolarization (-110 mV) from a holding potential of -50 mV. (A) Voltage-dependent current activated by 10 μM or 30 μM ATP. Current traces in the absence ($-\text{ATP}$) or presence ($+\text{ATP}$) of ATP are superimposed in each panel. (B) Contribution of the voltage-dependent current to total ATP-evoked current using different ATP concentrations. Mean values obtained from 4 oocytes in a standard extracellular solution containing 1.8 mM Ca^{2+} (\bullet) and an extracellular solution containing 10.8 mM Ba^{2+} (instead of Ca^{2+} ; \circ) were plotted. Bars represent the S.E.M. (C) Time course of activation of the voltage-dependent components. Time constants were determined as shown in Fig. 1B, and mean values obtained from 4 oocytes were plotted against holding potentials. Bars represent the S.E.M.

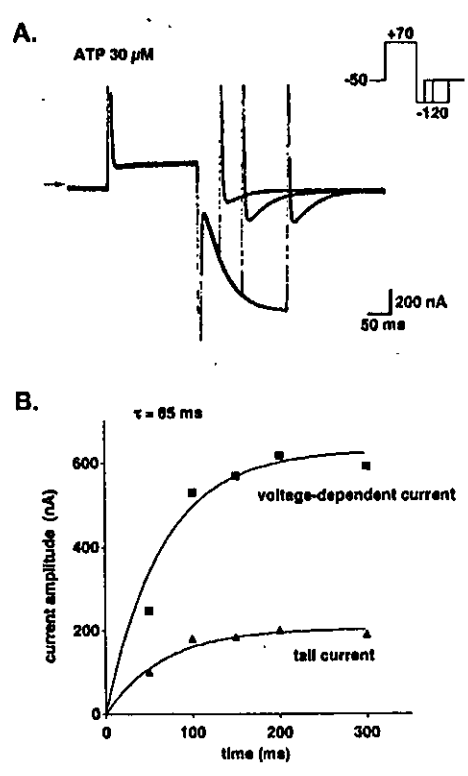


Fig. 4. Activation and tail current. (A) Gradual increase in magnitude of the tail current with increasing voltage-dependent current. Current traces obtained upon exposure to hyperpolarizing pulses (-120 mV) of different durations are superimposed. (B) Time course of activation of the voltage-dependent (■) and tail (▲) currents. Current amplitude was plotted against duration of hyperpolarization (also shown in panel A). The results of both time course activation experiments fit curves with a single time constant of 65 ms.

141 the relation between activation kinetics of the voltage-
 142 dependent component and time course of tail current. As
 143 shown in Fig. 4A, oocytes were stepped to 70 mV and
 144 then to -120 mV to induce the voltage-dependent
 145 component. When hyperpolarization at -120 mV was
 146 terminated after various periods, a gradual increase in
 147 amplitude of the tail current was observed with increased
 148 duration of hyperpolarization at -120 mV. Time courses
 149 of both the voltage-dependent component and tail current
 150 could be fitted with curves with a single time constant
 151 (65 ms in this case; Fig. 4B). Similar fitting with single
 152 time constants were made for 4 oocytes tested, and the
 153 mean time constant ± S.E.M. was 66.3 ± 2.4 ms.

154 With increased duration of the +70 mV depolarizing
 155 pulse, increased amplitude of the voltage-dependent
 156 component was observed at -120 mV (Fig. 5A). This
 157 may reflect "deactivation" of the voltage-dependent com-
 158 ponent (Scheme 1); where A is ATP, and R and R* are
 159 closed and open states, respectively, of the voltage-
 160 dependent component of P2X₂ receptor/channel. The
 161 deactivation time course could be fitted with a time
 162 constant of 70 ms in this case (Fig. 5B; mean ± S.E.M.,
 163 71.3 ± 1.3 ms; n=4).

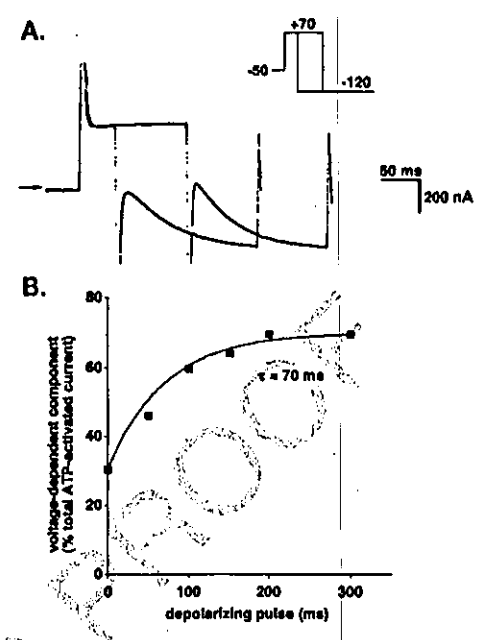


Fig. 5. Deactivation of the voltage-dependent component. (A) Current traces obtained using depolarizing pulses (+70 mV) of two different durations. The amplitude of the voltage-dependent component increased when the duration was prolonged. (B) Time course of deactivation of the voltage-dependent component. Current amplitude was plotted against duration of the depolarizing pulses (also shown in panel A).

3.4. Voltage dependence of activation and deactivation

164

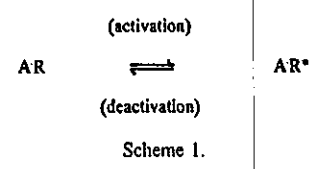
As shown in Fig. 1, contribution of the voltage-
 dependent component to total ATP-evoked current was
 influenced by the holding potential prior to hyperpolarization.
 This was further examined by testing a number of
 prepulses at various potentials prior to hyperpolarization
 (Fig. 6A). As the prepulse became more depolarized, a
 greater contribution of the voltage-dependent component to
 total ATP-evoked current was observed, and this contribu-
 tion became maximal near 0 mV (Fig. 6B). Thus, the
 voltage-dependent gate must be completely closed at
 potentials equal to or more positive than 0 mV. The data
 were fitted with a curve in accordance with the following
 model of "deactivation":

165
 166
 167
 168
 169
 170
 171
 172
 173
 174
 175
 176
 177

$$d_{\infty} = 1 / \{ 1 + \exp[(E_{1/2} - E_m) / k] \}, \quad (1)$$

where d_{∞} represents the relative proportion of closed gates
 at steady state, $E_{1/2}$ is the voltage at which the half-
 maximal closing occurs, E_m is the membrane potential, and

178
 180
 181



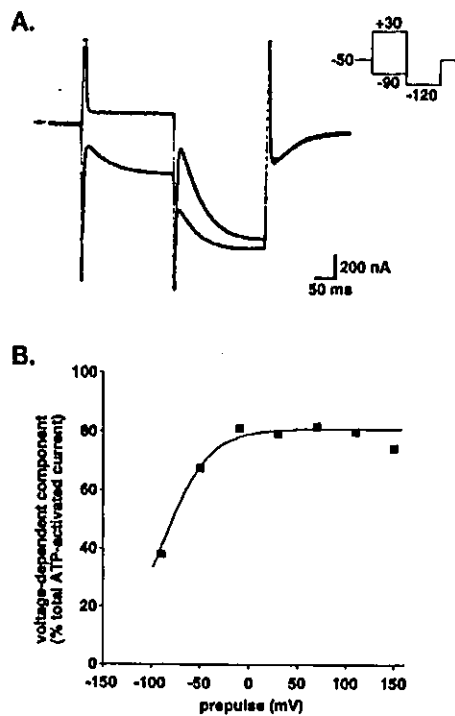


Fig. 6. Prepulse experiment. An ATP concentration of 30 μM was used. (A) Current traces obtained using prepulses of +30 mV ("a") or -90 mV ("b") prior to hyperpolarization at -120 mV. (B) Effect of prepulses. The relative contribution of the voltage-dependent current to total ATP-evoked current at -120 mV was plotted against each prepulse voltage. Some of this data is also shown in panel A.

182 k is a slope factor reflecting an energy barrier (Hodgkin and
183 Huxley, 1952; Hille, 1992a). As shown in Fig. 6B,
184 potential at which half the gates closed was estimated to
185 be -90 mV in this case (mean \pm S.E.M., -78.8 ± 5.2 mV;
186 $n=4$).

187 The voltage dependence of activation was also
188 examined. As shown in Fig. 7A, the channels responsible
189 for the voltage-dependent component was sufficiently
190 "deactivated" by applying a prepulse of +100 mV, and
191 they were then activated at various hyperpolarization
192 potentials. Contribution of the voltage-dependent compo-
193 nent to total ATP-evoked current decreased as the
194 hyperpolarization became more negative up to -45 mV
195 in the case shown in Fig. 7B. Potentials exceeding -45
196 mV could not be examined since the resultant ATP-
197 evoked current was not large enough to analyze. The data
198 were fitted in accordance with the following model of
199 "activation":

$$a_{\infty} = 1 / \{ 1 + \exp[(E_{1/2} - E_m) / k] \}, \quad (2)$$

200 where a_{∞} represents the degree of gate opening at steady
202 state. The other parameters are the same as those described
203 above. The data obtained using Eq. (2) (Fig. 7B) could be

204 fitted with a curve indicating that half of the gates were
205 open at a potential of -30 mV.

206 The above data suggest that activation of the voltage-
207 dependent gate occurs at more positive potentials than gate
208 deactivation. To further investigate this, the fraction of the
209 gates that escaped deactivation ($1-d_{\infty}$) was calculated from
210 the data obtained during deactivation experiments. The
211 deactivation data was then plotted alongside data obtained
212 from activation experiments (Fig. 7C). These data suggest
213 that the activation potential is 50 mV more positive than the
214 deactivation potential.

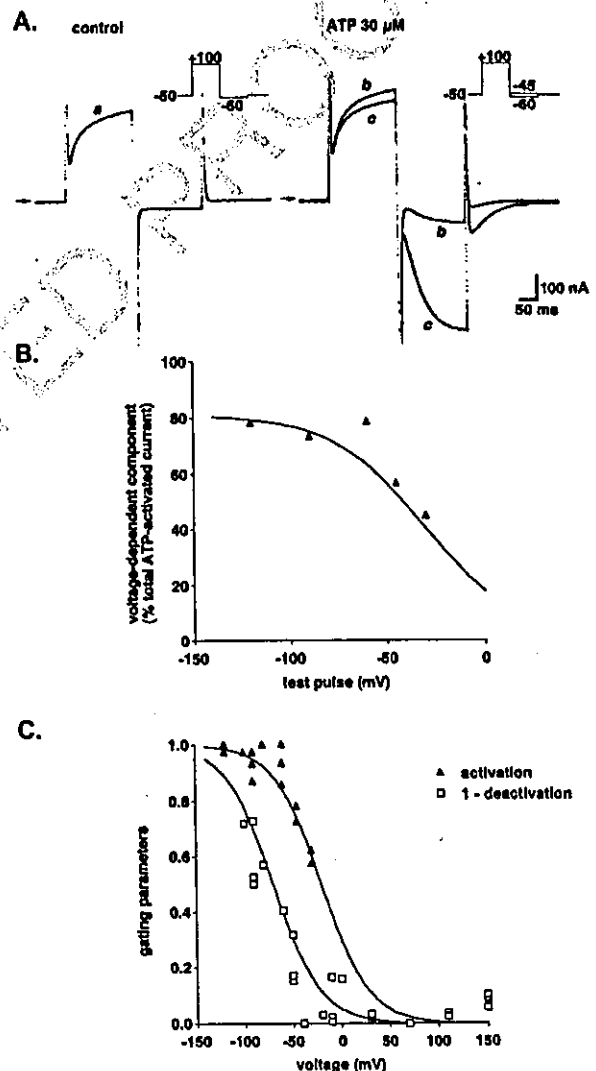
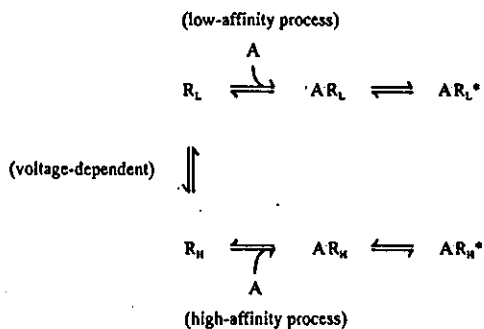


Fig. 7. Effect of hyperpolarization on voltage-dependent current. (A) Current traces before (control) and during the application of 30 μM ATP. In the panel on the right, two current traces obtained following hyperpolarization at -45 mV ("b") and -60 mV ("c") are superimposed. (B) Contribution of voltage-dependent current to total ATP-evoked current at various hyperpolarization potentials. Some of these data are shown in panel A. (C) Comparison of activation and deactivation. Parameters describing activation and deactivation were determined as described in the text. Each data point represents data obtained from individual oocytes.

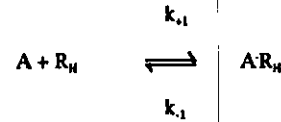
215 4. Discussion

216 4.1. Schematic model of voltage-dependent gating

217 Recombinant P2X₂ receptor/channels expressed in *Xenopus* oocytes exhibited voltage-dependent gating properties similar to those of the channels in PC12 cells (Nakazawa et al., 1997b). The following similarities were observed: (1) the gate opens at negative potentials, (2) activation follows a time course with a time constant of 40 to 70 ms, and (3) gating depends on ATP concentrations. Thus, voltage-dependent gating in PC12 cells may be due to intrinsic expression of P2X₂ receptor/channels. We depict here a model that has been proposed to explain voltage-dependent gating of the channels in PC12 cells (Scheme 2), where A is ATP, R_L and R_H represent closed states, and R* represents the open state (Nakazawa et al., 1997b). In this model, voltage-dependent gating is explained by transition between low and high ATP-affinity states. Upon hyperpolarization, there is a shift from the R_L to the R_H conformation. ATP preferentially binds to channels in the R_H state (A·R_H), after which the channels open (A·R_H*). Binding of ATP is the rate-limiting step since activation kinetics were observed to depend on ATP concentrations in the present study (Fig. 3C). The following rate constants have been proposed (Scheme 3): where k_{+1} parallels the concentration of ATP ($k_{+1}=k'_{+1}[ATP]$), and K_d is given by k_{-1}/k'_{+1} (Hille, 1992b). In the present experiment, an activation time constant of 65 ms was observed in the presence of 30 μM of ATP (Fig. 4), which is equivalent to a rate constant of 15 s⁻¹. Using these values, $k'_{+1}=k_{+1}/[ATP]=15\text{ s}^{-1}/(30\text{ }\mu\text{M})=5\times 10^5\text{ M}^{-1}\text{ s}^{-1}$. An inactivation time constant of 70 ms was observed in the presence of 30 μM of ATP (Fig. 5), which is equivalent to a rate constant of 14 s⁻¹. Thus, K_d was calculated to be $k_{-1}/k'_{+1}=14\text{ s}^{-1}/(5\times 10^5\text{ M}^{-1}\text{ s}^{-1})=28\text{ }\mu\text{M}$, which is slightly less than the EC₅₀ value obtained at -50 mV (about 40 μM). This estimation is in accordance with the finding that the voltage-dependent component is not completely activated at -50 mV (Fig. 7C). It is difficult to quantify the low-affinity ATP binding state since the relationship between concentration and response needs to be assessed at highly positive potentials, while P2X₂ receptor/channels permit only small current due to their inward-rectifying



Scheme 2.



Scheme 3.

256 nature. We estimate here the low affinity from simple theoretical concentration-response curves. Fig. 8 shows two concentration-response curves. One demonstrates an EC₅₀ of 30 μM, corresponding to a high-affinity state. If the other low-affinity state demonstrates an EC₅₀ of 100 μM, more P2X₂ receptor/channels were in the high-affinity state in the presence of 10 μM ATP, and more were in the low-affinity state in the presence of 300 μM ATP. This is consistent with the greater observed contribution of the voltage-dependent component to total ATP-evoked current in the presence of 10 μM, while little was observed in the presence of 300 μM ATP (Fig. 3). Thus, the low-affinity state may be lower than the high-affinity state by threefold or larger.

257 The idea of the transition of P2X₂ receptor/channels between low- and high-affinity states might explain the "non-voltage-dependent" component of ATP-evoked current. For example, the current evoked by 30 μM ATP was not completely observed as voltage-dependent component even when activated at very negative potentials (Fig. 7B) or following deactivation at very positive potentials (Fig. 6B). This "non-voltage-dependent current" (about 20% of the total ATP-evoked current) might result from the activation of P2X₂ receptor/channels in the low-affinity state prior to voltage-dependent activation.

269 The voltage dependence of activation and deactivation differed, with deactivation occurring at more negative potentials (Fig. 7C). This indicates that the activation and the deactivation do not arise from a simple reversible "back-and-forth" process, rather, two voltage-dependent processes

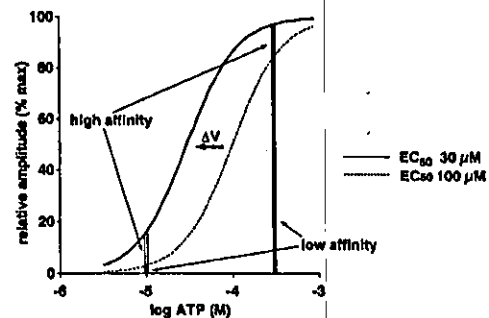
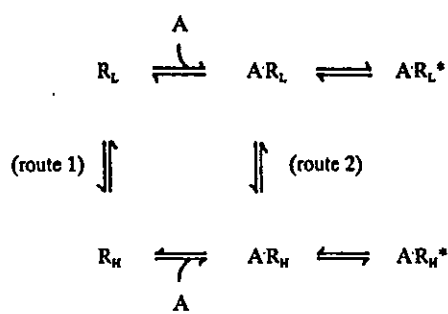


Fig. 8. Voltage-dependent change in sensitivity to ATP might explain dependence of the voltage-dependent current on ATP concentration. Low-affinity (EC₅₀=100 μM) and high-affinity (EC₅₀=30 μM) states of the receptor are thought to exist (Hill coefficient; 1.5). Each receptor shifts from a low-affinity to a high-affinity state upon hyperpolarization (ΔV). With 10 μM ATP, only a small proportion of the receptors, many of which were in the low-affinity state, were activated prior to hyperpolarization, but many more were activated upon induction of the high-affinity state by hyperpolarization. In the presence of 300 μM ATP, a larger proportion of the receptors were activated even in the low-affinity state, and induction of the high-affinity state caused only a marginal increase in activated receptors.



Scheme 4.

285 may be involved. We propose the following modification to
286 Scheme 2.

287 This model (Scheme 4) involves two voltage-dependent
288 processes, one resulting in activation through "route 1", and
289 the other resulting in deactivation through "route 2". Such
290 model would explain the observed difference in voltage
291 dependence between activation and deactivation. However,
292 we would expect this model to result in more difficult to
293 interpret data than we did above based on Schemes 2 and 3.

294 4.2. Relevance of voltage-dependent gating

295 P2X₂ receptor is expressed in a number of neurons (e.g.,
296 Atkinson et al., 2000; Rubio and Soto, 2001). P2X₂
297 receptor/channel is permeable to Ca²⁺ (Egan and Khakh,
298 2004), and Ca²⁺ influx through the channel may influence
299 cellular activity, although its exact role remains to be
300 clarified. The voltage-dependent gating reported here may
301 be relevant to the Ca²⁺ influx from the following consid-
302 eration. Na⁺ current (*I*_{Na}) and Ca²⁺ current (*I*_{Ca}) permeating
303 through P2X₂ receptor/channel are:

$$I_{Na} = -P_{Na} \frac{E_m F^2}{RT} \frac{[Na]_o}{1 - \exp(-EF/RT)} \quad (3)$$

$$I_{Ca} = -4P_{Ca} \frac{E_m F^2}{RT} \frac{[Ca]_o \exp(-2EF/RT)}{1 - \exp(-2EF/RT)}, \quad (4)$$

304
305 where *P*_{Na} and *P*_{Ca} represent the permeability of Na⁺ and
306 Ca²⁺, respectively, *E*_m represents the membrane potential,
307 and *F*, *R*, and *T* are their usual physicochemical meanings
308 (Fatt and Ginsborg, 1958; Nakazawa et al., 1989). The ratio
309 of *I*_{Na} to *I*_{Ca} is thus:
310

$$\frac{I_{Ca}}{I_{Na}} = \frac{4P_{Ca}[Ca]_o}{P_{Na}[Na]_o} \frac{1}{\exp(E_m F/RT)[\exp(E_m F/RT) + 1]} \quad (5)$$

311 This equation indicates that the ratio of *I*_{Ca}/*I*_{Na} is larger at
312 more negative potentials. The ratio calculated at -90 mV is
313 about 13-fold larger than that calculated at -30 mV. Thus,
314 channel opening at negative potentials favors Ca²⁺ over Na⁺
315 influx. Thus, voltage-dependent gating may facilitate
316 cellular Ca²⁺-dependent responses when cells are hyper-
317 polarized. This may occur when efflux through K⁺ channels
318
319

outpaces depolarization afforded by opening of P2X₂ 320
receptor/channels. 321

4.3. Conclusion 322

The results of the present study suggested that P2X₂ 323
receptor exhibits voltage-dependent gating, and that this is 324
not due to simple activation and deactivation of a single 325
gate, but rather, due to a transition from a low ATP affinity 326
to a high ATP affinity state. This may favor Ca²⁺ influx at 327
negative potentials, although further studies are required to 328
clarify the physiological significance of voltage-dependent 329
gating of P2X₂ receptor. 330

Acknowledgements 331

This work was supported, in part, by a Health and 332
Labour Science Research Grant for Research on Advanced 333
Medical Technology from the Ministry of Health, Labour 334
and Welfare, Japan, as well as a grant-in-aid for scientific 335
research from the Ministry of Education, Science, Sports 336
and Culture, Japan (KAKENHI 13672319) awarded to K.N. 337

References 338

- 339
340 Atkinson, L., Batten, T.F., Deuchars, J., 2000. P2X₂ receptor immuno-
341 reactivity in the dorsal vagal complex and area postrema of the rat.
342 *Neuroscience* 99, 683-696.
343 Brake, A.J., Wagenbach, M.J., Julius, D., 1994. New structural motif for
344 ligand-gated ion channels defined by an ionotropic ATP receptor.
345 *Nature* 371, 519-523.
346 Clyne, J.D., LaPointe, L.D., Hume, R.I., 2002. The role of histidine
347 residues in modulation of the rat P2X₂ purinoceptor by zinc and pH.
348 *J. Physiol.* 539, 347-359.
349 Egan, T., Khakh, B.S., 2004. Contribution of calcium ions to P2X channel
350 responses. *J. Neurosci.* 24, 3413-3420.
351 Egan, T.M., Haines, W.R., Voigt, M.M., 1998. A domain contributing to the
352 ion channel of ATP-gated P2X₂ receptors identified by the substituted
353 cysteine accessibility method. *J. Neurosci.* 18, 2350-2359.
354 Ennion, S., Hagan, S., Evans, R.J., 2000. The role of positively charged
355 amino acids in ATP recognition by human P2X₁ receptors. *J. Biol.*
356 *Chem.* 275, 29361-29367.
357 Fatt, P., Ginsborg, B.L., 1958. The ionic requirements for the production of
358 action potentials in crustacean muscle fibres. *J. Physiol.* 142, 516-543.
359 Haines, W.R., Migita, K., Cox, J.A., Egan, T.M., Voigt, M.M., 2001. The
360 first transmembrane domain of the P2X receptor subunit participates
361 in the agonist-induced gating of the channel. *J. Biol. Chem.* 276,
362 32793-32798.
363 Hille, B., 1992a. Classical biophysics of the squid giant axon. Ionic
364 channels of excitable membranes, Second Edition. Sinauer, Sunderland,
365 MA, pp. 23-58.
366 Hille, B., 1992b. Ligand-gated channels of fast chemical synapses. Ionic
367 channels of excitable membranes, Second Edition. Sinauer, Sunderland,
368 MA, pp. 140-169.
369 Hodgkin, A.L., Huxley, A.F., 1952. The dual effect of membrane potential
370 on sodium conductance in the giant axon of *Loligo*. *J. Physiol.* 116,
371 497-506.
372 Jiang, L.H., Rassendren, F., Surprenant, A., North, R.A., 2000. Identifi-
373 cation of amino acid residues contributing to the ATP-binding site of a
374 purinergic P2X receptor. *J. Biol. Chem.* 275, 34190-34196. 374

- 375 Jiang, L.H., Rassendren, F., Spelta, V., Surprenant, A., North, R.A., 2001. Amino acid residues involved in gating identified in the first membrane-spanning domain of the rat P2X₂ receptor. *J. Biol. Chem.* 276, 14902–14908.
- 379 Khakh, B.S., 2001. Molecular physiology of P2X receptors and ATP signalling at synapses. *Nat. Rev.* 2, 165–174.
- 381 Migita, K., Haines, W.R., Voigt, M.M., Egan, T.M., 2001. Polar residues of the second transmembrane domain influence cation permeability of the ATP-gated P2X₂ receptor. *J. Biol. Chem.* 276, 30934–30941.
- 384 Nakazawa, K., Ohno, Y., 1997. Effects of neuroamines and divalent cations on cloned and mutated ATP-gated channels. *Eur. J. Pharmacol.* 325, 101–108.
- 387 Nakazawa, K., Fujimori, K., Takanaka, A., Inoue, K., 1989. An ATP-activated conductance in pheochromocytoma cells and its suppression by extracellular calcium. *J. Physiol.* 428, 257–272.
- 390 Nakazawa, K., Liu, M., Inoue, K., Ohno, Y., 1997a. pH dependence of facilitation by neurotransmitters and divalent cations of P2X₂ purinoceptor/channels. *Eur. J. Pharmacol.* 337, 309–314.
- 393 Nakazawa, K., Liu, M., Inoue, K., Ohno, Y., 1997b. Voltage-dependent gating of ATP-activated channels in PC12 cells. *J. Neurophysiol.* 78, 884–890.
- Nakazawa, K., Ojima, H., Ohno, Y., 2002. A highly conserved tryptophane residue indispensable for cloned rat neuronal P2X receptor activation. *Neurosci. Lett.* 324, 141–144.
- North, R.A., 2002. Molecular physiology of P2X receptors. *Physiol. Rev.* 82, 1013–1067.
- Ralevic, V., Burnstock, G., 1998. Receptors for purines and pyrimidines. *Pharmacol. Rev.* 50, 413–492.
- Rassendren, F., Buell, G., Newbolt, A., North, R.A., Surprenant, A., 1997. Identification of amino acid residues contributing to the pore of a P2X receptor. *EMBO J.* 16, 3446–3454.
- Roberts, J.A., Evans, R.J., 2004. ATP binding at human P2X₁ receptors. Contribution of aromatic and basic amino acids revealed using mutagenesis and partial agonists. *J. Biol. Chem.* 279, 9043–9055.
- Rubio, M., Soto, F., 2001. Distinct localization of P2X receptors at excitatory postsynaptic specializations. *J. Neurosci.* 21, 641–653.
- Weber, W.-M., 1999. Ion currents of *Xenopus laevis* oocytes: state of the art. *Biochim. Biophys. Acta* 1421, 213–233.
- Zhang, Y., Hamill, O.P., 2000. Calcium, voltage- and osmotic stress sensitive currents in *Xenopus* oocytes and their relationship to single mechanically gated channels. *J. Physiol.* 523, 83–99.

416

UNCORRECTED PROOF

Amino acid substitutions from an indispensable disulfide bond affect P2X₂ receptor activation

Ken Nakazawa^{a,*}, Hiloe Ojima^{a,b}, Reiko Ishii-Nozawa^b, Koichi Takeuchi^b, Yasuo Ohno^c

^aCellular and Molecular Pharmacology Section, Division of Pharmacology, National Institute of Health Sciences, 1-18-1 Kamiyoga, Setagaya, Tokyo 158-8501, Japan

^bDepartment of Clinical Pharmacology, Meiji Pharmaceutical University, Kiyose, Tokyo 204-8588, Japan

^cDivision of Pharmacology, National Institute of Health Sciences, 1-18-1 Kamiyoga, Setagaya, Tokyo 158-8501, Japan

Received 17 July 2003; received in revised form 2 October 2003; accepted 7 October 2003

Abstract

The roles of six amino acid residues downward from an extracellular disulfide bond involving Cys²²⁴ in rat P2X₂ receptor were examined. When Cys²²⁴ or Pro²²⁵ was replaced with alanine, the responsiveness to ATP was lost. When Ile²²⁶ was replaced with other hydrophobic amino acids, the responsiveness to ATP was reduced or abolished. When Phe²²⁷ was replaced with leucine or isoleucine, the responsiveness to ATP was abolished. The responsiveness to ATP was moderately decreased with the alanine-substitution for Arg²²⁸ and it was markedly decreased with the alanine-substitution for Leu²²⁹. As for the alanine-substitution for Gly²³⁰, the sensitivity was changed, but the maximal response to ATP was not reduced. The results suggested that a precise structure is required for amino acid residues close to the disulfide bond and, in general, the amino acid residues at odd number positions and those closer to the disulfide bond are more influential to the ATP responsiveness.

© 2003 Elsevier B.V. All rights reserved.

Keywords: P2X receptor; ATP; Site-directed mutagenesis; *Xenopus* oocyte; Membrane current

1. Introduction

P2X receptors are ion channel-forming membrane proteins that are activated by extracellular ATP (see reviews, Khakh, 2001; North, 2002). One functional ion channel is presumably formed by three homogenous subunits. Each subunit has two transmembrane regions (TM1 and TM2) and a long extracellular loop (E1) between them. Basic amino acid residues near the outer mouth of the channel pore formed by TM1 and TM2 appear to serve as a part of the binding pocket of ATP molecules (Ennion et al., 2000; Jiang et al., 2000). In addition to these basic residues, amino acid residues in E1 apart from the channel pore have been shown to affect the channel activation by ATP. P2X₂ receptor did not respond to ATP when Gly²⁴⁷ in E1 was replaced with alanine (Nakazawa and Ohno, 1999).

The sensitivity to ATP was reduced when Gly²⁴⁸ was replaced with valine and the responsiveness was lost when the residue was replaced with leucine (Nakazawa et al., 2002). The replacement of Trp²⁵⁶ with other amino acid residues except for tyrosine also resulted in the loss of responsiveness (Nakazawa et al., 2002). These results suggest that the structure around these positions should be precisely maintained for the channel activation by ATP. Recently, the pairs of cysteines that form disulfide bonds have been identified for P2X₁ (Ennion and Evans, 2002) and P2X₂ (Clyne et al., 2002) receptors. Among these cysteines, the structure formed by Cys²²⁴ through a disulfide bond with Cys²¹⁴ appears to be critical because the replacement of this residue with alanine was non-functional (Clyne et al., 2002). Cys²²⁷ in P2X₁, which corresponds to Cys²²⁴ in P2X₂ (see Fig. 1), may also play an indispensable role in the formation of such a structure because its alanine substitution resulted in about 50-fold reduction in the sensitivity to ATP (Ennion and Evans, 2002). In the present study, we examined the roles of amino acid residues following Cys²²⁴ in P2X₂ receptor to understand

* Corresponding author. Tel.: +81-3-3700-9704; fax: +81-3-3707-6950.

E-mail address: nakazawa@nih.go.jp (K. Nakazawa).

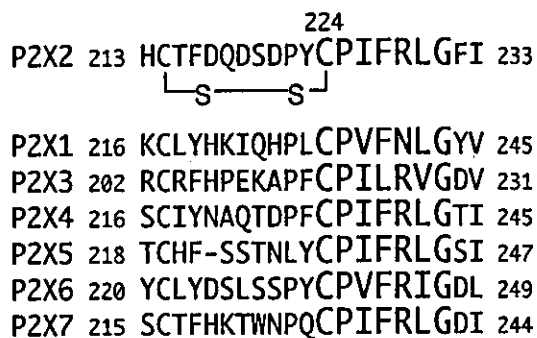


Fig. 1. Amino acid sequence near Cys²²⁴ in the extracellular loop of P2X₂ receptor and corresponding sequences of P2X receptor subclasses. Amino acid residues targeted for site-directed mutagenesis and those in the equal positions were shown as the larger characters. Cys²²⁴ forms a disulfide bond with Cys²¹⁴.

structural requirements for the channel activation in this region.

2. Materials and methods

2.1. Oocyte expression and membrane current measurements

The expression of cloned and mutant P2X₂ receptor and the recordings of ionic current through the channels were performed according to our previous report (Nakazawa et al., 1998). Briefly, P2X₂ receptor mutants were constructed from the cloned P2X₂ receptor (Brake et al., 1994) by site-directed mutagenesis. Amino acid residues targeted for mutagenesis were shown in Fig. 1. The wild-type and the mutant channels were expressed in *Xenopus* oocytes for a 4-day incubation at 18 °C and the oocytes were served for membrane current measurements. Oocytes were bathed in ND96 solution containing (in mM) NaCl 96, KCl 2, CaCl₂ 1.8, MgCl₂ 1, HEPES 5 (pH 7.5 with NaOH). ATP (adenosine 5'-triphosphate disodium salt; Sigma, St. Louis, MO, USA) was applied by superfusion for about 6 s with a regular interval of 1 min.

2.2. Immunoblotting analysis

The expression of channel protein was confirmed by immunoblotting analysis. Crude membrane fractions were prepared from oocytes (20 oocytes for the wild-type channel and each mutant) according to Newbolt et al. (1998) with minor modifications. Oocytes were suspended in a 50 × stock of a protease and phosphatase inhibitor cocktail (Sigma, general use; 1 bottle for 100 ml effective solution) diluted in a buffer containing 20 mM Tris-HCl, 2 mM EDTA (disodium salt), 0.5 mM EGTA and 320 mM sucrose by pipetting. The homogenate was horizontally shaken at 100 rpm for 15 min at 4 °C and then centrifuged at 14,000 rpm for 2 min. The supernatants were analyzed by SDS-

PAGE gel electrophoresis and immunoblotting. By using P2X₂ receptor antibodies (Oncogene, Boston, MA, USA) and anti-rabbit Ig, horseradish peroxidase-linked whole antibody (from donkey; Amersham, Little Chalfont, England), correct channel expression was detected as a 65-kDa band.

2.3. Data analysis

Parameters for ATP sensitivity (EC₅₀, pD₂ and Hill coefficient) were obtained from current responses using the following equation:

$$E = E_{\max} A^n / [A^n + (EC_{50})^n], \quad (1)$$

where E is an effect (current response), E_{\max} is a maximal response, A is ATP concentration, EC_{50} is concentration required for a half-maximal effect and n is a Hill coefficient (slope factor). When EC_{50} and n were calculated from ATP concentrations used and obtained current responses, Eq. (1) was transformed to:

$$\log[E/(E_{\max} - E)] = n(\log A - \log EC_{50}), \quad (2)$$

and linear regression was made using Microsoft® Excel X. pD₂ values were negative logarithm of EC₅₀ values. When experimental data were fitted by a two binding-site model, the fraction of one binding-site (f) and that of the other binding-site ($1-f$) were introduced. The effect mediated through each binding-site was calculated from Eq. (1) and the fraction (f or $1-f$), and the sum of these effects was obtained.

3. Results

3.1. Amino acid substitutions and ATP responsiveness

Cys²²⁴ and neighboring Pro²²⁵ are completely conserved among seven subclasses of P2X receptors (Fig. 1; Soto et al., 1997). Fig. 2 shows concentration–response relationship for ATP-evoked current recorded from oocytes expressing the wild-type P2X₂ receptor and the Cys²²⁴- or Pro²²⁵-to-alanine-substituted mutants (C224A or P225A, respectively). C224A exhibited no current response to ATP, as has been reported by Clyne et al. (2002). P225A also failed to respond to ATP. To examine the effects of amino acid residues succeeding to Pro²²⁵, we first constructed deletion mutants. When three residues next to Pro²²⁵ (Ile²²⁶, Phe²²⁷ and Arg²²⁸) were deleted, the responsiveness to ATP was lost. Deletion of the former two or even Ile²²⁶ alone also resulted in the loss of the responsiveness. The preliminary results suggest that these amino acid residues also appeared to be essential. Thus, instead of deletion, we introduced amino acid substitutions to these residues in a one-by-one manner.

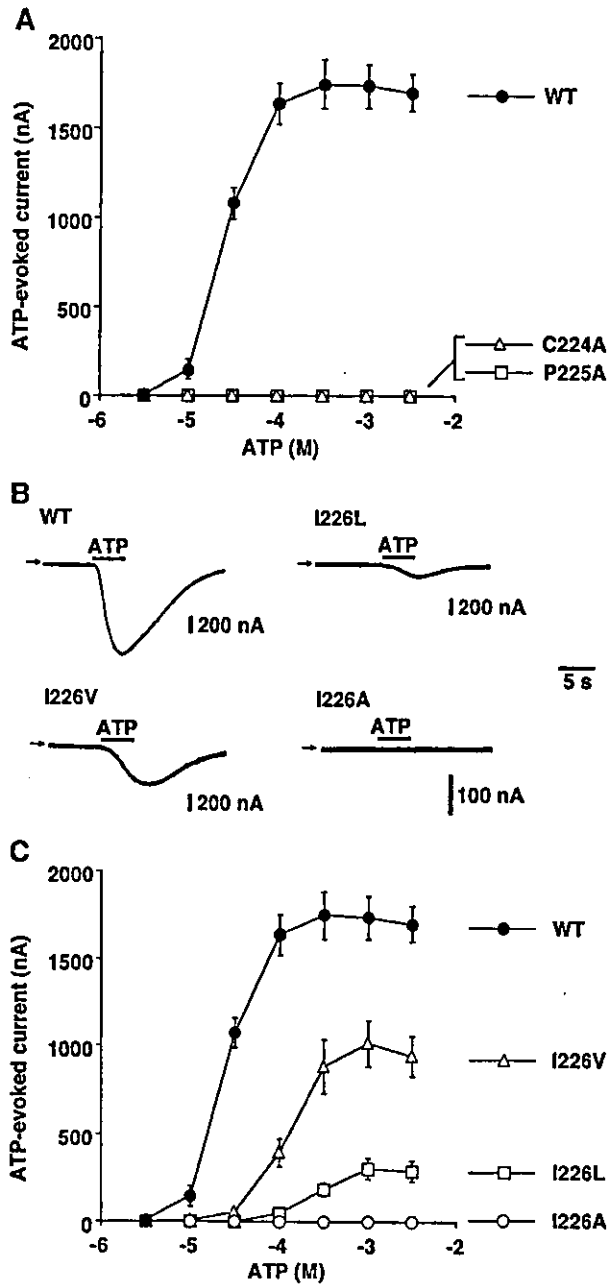


Fig. 2. (A) Disappearance of current responses to ATP by the replacement of Cys²²⁴ or Pro²²⁵ with alanine (C224A or P225A). Peak amplitude of currents activated by ATP at -50 mV was plotted against ATP concentrations. Each symbol and bar represent mean and S.E. obtained from five to eight oocytes. In contrast to current responses in oocytes expressing the wild-type channel (WT), no response was observed in those expressing the mutant channels. (B) Currents activated by $30 \mu\text{M}$ ATP in oocytes expressing the wild-type (WT) and Ile²²⁶-to-leucine (I226L), -valine (I226V) and -alanine (I226A)-substituted mutant channels. The oocytes were held at -50 mV. Arrows indicate zero current levels. (C) Concentration–response relationship for the wild-type and Ile²²⁶-replaced channels. The current responses were obtained as shown in B. The concentration–response relationship for the wild-type channel (WT) was also shown for comparison. Each symbol and bar represent mean and S.E. obtained from five to eight oocytes.

Ile²²⁶ was replaced with hydrophobic amino acid residues because this position was occupied by isoleucine or valine in seven P2X receptor subclasses (Fig. 1). Fig. 2B shows current responses to $100 \mu\text{M}$ ATP in oocytes expressing the wild-type and the mutant channels. When substituted with leucine, which has a volume similar to that of isoleucine (Chothia, 1975), the ATP-evoked current was markedly reduced (Fig. 2B,C; I226L). When substituted with valine, a smaller hydrophobic residue, the reduction of the current

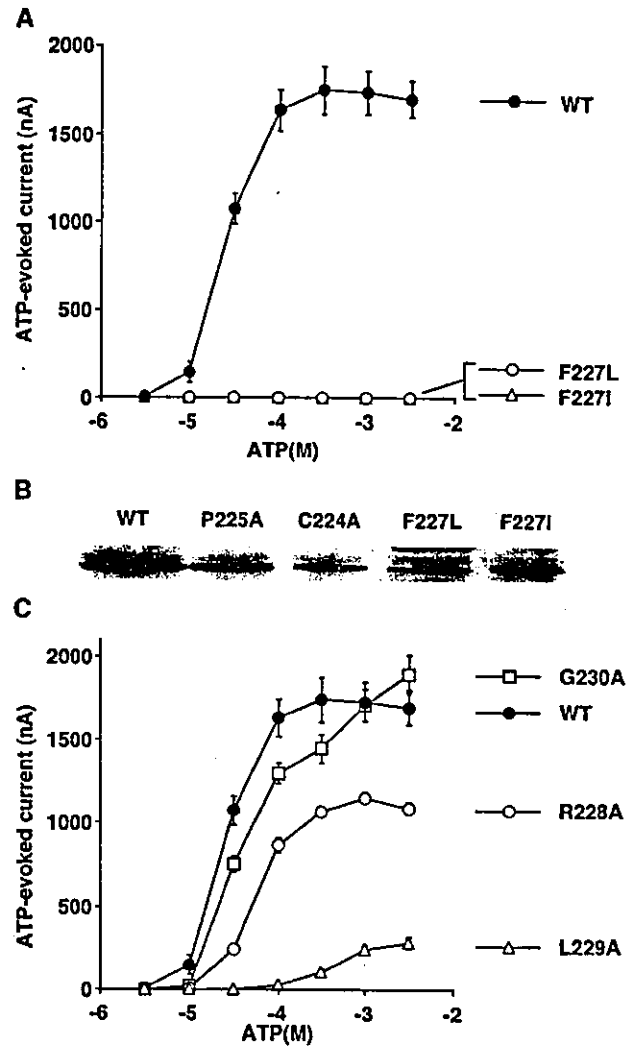


Fig. 3. (A) Disappearance of current responses to ATP by the replacement of Phe²²⁷ with leucine (F227L) or isoleucine (F227I). Data obtained from five to eight oocytes were shown as in Fig. 2A. (B) Immunoblotting analysis using anti-P2X₂ receptor antibody. A section corresponding to P2X₂ receptor protein (about 65 kDa) was shown to compare the expression in membrane fractions prepared from the oocytes injected with the wild-type channel (WT) and four non-ATP responsive mutants shown in Fig. 2A (C224A and P225A) and A of this figure (F227L and F227I). (C) Concentration–response relationship for the wild-type and Arg²²⁸- (R228A), Leu²²⁹- (L229A) and Gly²³⁰-to-alanine-substituted mutants. The concentration–response relationship for the wild-type channel (WT) was also shown for comparison. Data obtained from five to eight oocytes were shown as in Fig. 2A.

was less remarkable than in the case of the leucine-substitution (Fig. 2B,C; I226V). When substituted with alanine, a hydrophobic residue smaller than valine, the current responsiveness to ATP was abolished (Fig. 2B,C; I226A).

Phe²²⁷, a residue succeeding to Ile²²⁶, is conserved among six of seven P2X receptor subclasses (Fig. 1). In the remaining subclass (P2X₃), leucine is present instead of phenylalanine. When Phe²²⁷ was replaced with leucine, the current response to ATP disappeared (Fig. 3A; F227L). The current response has also disappeared when replaced with isoleucine (Fig. 3A; F227I). The disappearance of the current response may not be due to non-expression of receptor protein because the protein expression of F227L or F227I was confirmed by immunoblotting analysis (Fig. 3B). The protein expression was also confirmed for the C224A, P225A (Fig. 3B) or I226A (not shown).

Three residues succeeding to Phe²²⁷ were alanine-substituted (Fig. 3C). The current response to ATP was reduced to about 60% when Arg²²⁸ was replaced with alanine (R228A). The current response was, however, much reduced (to about 20%) when Leu²²⁹ was replaced with alanine (L229A). As for the replacement of Gly²³⁰, the

maximal current response was comparable to that with the wild-type channel (G230A).

3.2. Sensitivities to ATP

To compare the sensitivity to ATP, the concentration–response data were normalized to the maximal response (Fig. 4). Theoretical curves were fitted to the normalized data (see Section 2), and EC₅₀ values and Hill coefficients were determined. For the wild-type channel, the EC₅₀ value was 29 μM and the Hill coefficient was 2.3. Ile²²⁶-, Arg²²⁸- and Leu²²⁹-substituted mutants exhibited lower sensitivities to ATP than the wild-type channel did (Fig. 4A–C), and the order of the sensitivities was R228A>I226V ≈ I226L>L229A. Hill coefficients for these mutants (varying from 1.7 to 2.6) were similar to that for the wild-type channel. When the curve fitting was applied to the data with G230A, the Hill coefficient as well as the ATP-sensitivity was lower than those for the wild-type channel (Fig. 4D, solid curve). The data points in Fig. 4D were, however, not well fitted to the solid curve. In fact, a regression coefficient of the fitting for the G230A

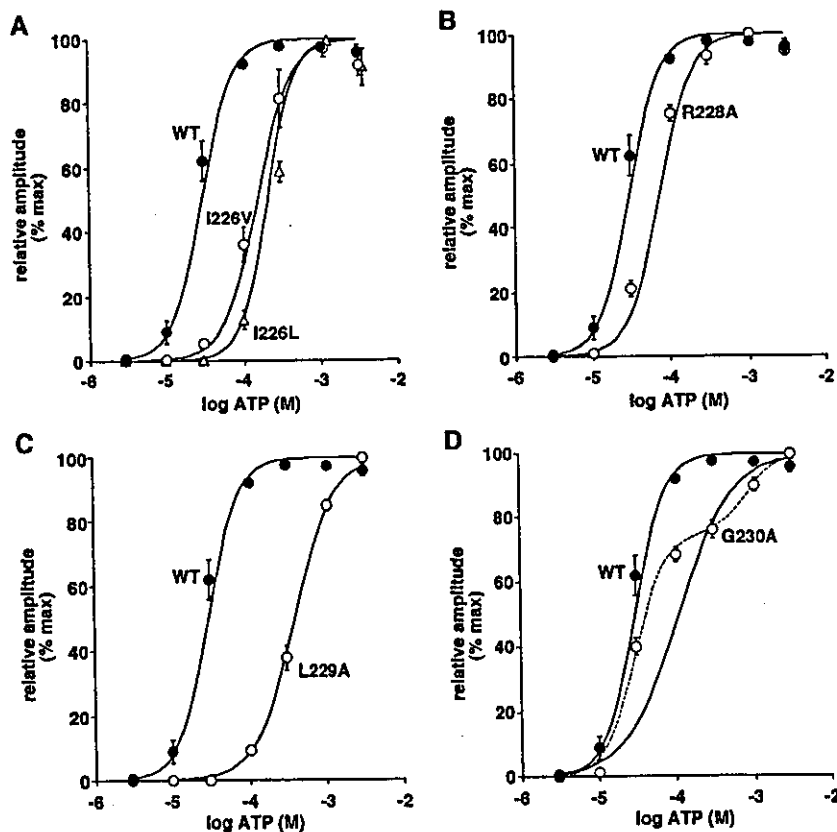


Fig. 4. (A–C) Curve-fittings to concentration–response data for the wild-type and the mutant channels. Current responses to ATP were normalized to maximal responses in individual oocytes and mean values were plotted against ATP concentrations. A curve was fitted to data assuming a homogenous binding-site for each channel type as shown in Section 2. Bars are S.E. Parameters calculated and used for fittings are: EC₅₀ (in μM); 29 (WT), 151 (I226V), 202 (I226L), 72 (R228A), 379 (L229A), 108 (G230A); Hill coefficient; 2.3 (WT), 2.0 (I226V), 2.6 (I226L), 2.1 (R228A), 1.7 (L229A), 1.3 (G230A). (D) Curve-fittings to concentration–response data for G230A mutants. The data and were shown and the solid curve with an EC₅₀ value of 108 μM and a Hill coefficient of 1.3 was fitted to the data as in A–C. For the broken curve, it was constructed assuming 75% of binding sites are equivalent to the wild-type receptor and the remaining 25% of binding sites have a lower affinity (EC₅₀; 800 μM) and the same slope (Hill coefficient; 2.3).

($r=0.91$) was markedly smaller than those for the remaining channels (0.98–1.00). The poor fitting suggests that this simple theoretical fitting was not available for G230A. Thus, a fitting was made assuming two independent binding sites (Fig. 4D, broken curve). A curve could be fitted with the data when assuming that 75% of the current response is mediated through a binding site having the same EC_{50} and Hill coefficient as the wild-type channel does, and the remaining 25% is mediated through another binding site having the same Hill coefficient but a larger EC_{50} value (800 μ M).

3.3. ATP responsiveness and amino acid positions

In Fig. 4, we used the mean values for the curve fittings. Similar curve fittings were applied to data obtained from individual oocytes, and sensitivities to ATP were determined. pD_2 values obtained in this manner as well as the maximal current responses were plotted for the wild-type and the mutant channels in Fig. 5. For the channels with which the current responses to ATP were observed, a clear correlation was found between the maximal current amplitude and the ATP sensitivity; the channels having exhibited smaller maximal current amplitude exhibited lower sensitivity to ATP. In the amino acid sequence beginning from Ile²²⁶ to Gly²³⁰, the substitution of an amino acid residue at an odd number position resulted in larger changes than that at an even number position. For example, the substitution of Phe²²⁷ resulted in the loss of ATP responsiveness, whereas the substitution of Ile²²⁶ or Arg²²⁸ did not lose the responsiveness in most cases. Similarly, the substitution of Leu²²⁹ resulted in large decreases in both the maximal amplitude and the ATP sensitivity, but the substitution of Arg²²⁸ or Gly²³⁰ resulted in relatively small decreases in these indexes. Within the odd or even number positions, the substitution of

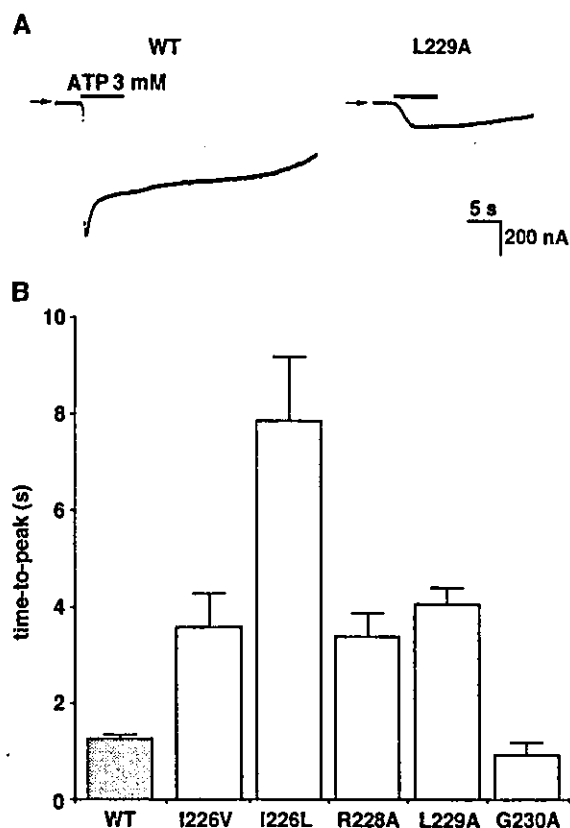


Fig. 6. Activation time course of ATP-evoked current through the wild-type and mutant channels. (A) Currents activated by 3 mM ATP in oocytes expressing the wild-type (WT) and L229A mutant channels. The oocytes were held at -50 mV. Arrows indicate zero current levels. (B) Comparison of time required for peak current evoked by 3 mM ATP ("time-to-peak"). Each column and bar represent mean and S.E. obtained from five to eight oocytes.

an amino acid residue closer to the disulfide bond involving Cys²²⁴ resulted in larger changes in the ATP responsiveness. The substitutions of Phe²²⁷ resulted in the loss of the

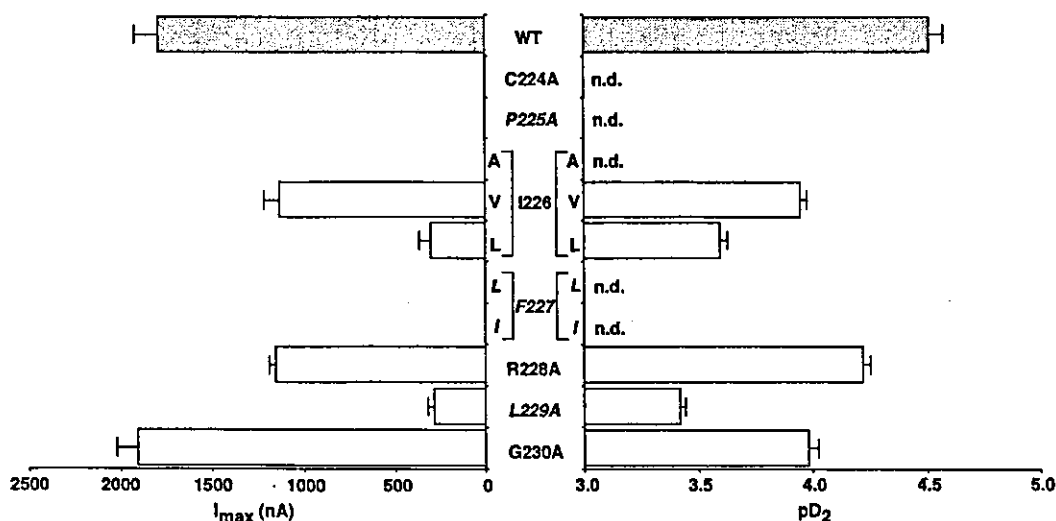


Fig. 5. Comparison of the maximal current amplitude (I_{max}) and the sensitivity to ATP (pD_2) among the wild-type and the mutant channels. The parameters were calculated from each oocytes and mean values were shown for each channel type. Bars are S.E. n.d.: not determined because of the loss of the ATP responsiveness.

responsiveness, whereas the substitution of Leu²²⁹ resulted in large decreases in the indexes for the responsiveness, but not in the loss of responsiveness. As for the amino acid substitutions at the even number positions, the order of the maximal current responses was Gly²³⁰>Arg²²⁸>Ile²²⁶ though the ATP sensitivities were comparable between Arg²²⁸ and Gly²³⁰.

3.4. Activation kinetics

When ATP was applied, activation kinetics was generally faster for the wild-type channel than that for the low responsiveness mutants such as I226V or L229A. To compare the activation kinetics quantitatively, we measured the time required for peak current amplitude when activated by 3 mM ATP ("time-to-peak"; Fig. 6). The time-to-peak was <2 s for the wild-type channel, whereas it was >3 s for the low responsiveness mutants (I226V, I226L, R228A and L229A). The time-to-peak for G230V was similar to that for the wild-type channel.

4. Discussion

We have examined the effects of amino acid substitutions downward from Cys²²⁴ in the extracellular loop of P2X₂ receptor. When Cys²²⁴ was replaced with alanine, the responsiveness to ATP was lost (Fig. 2A), suggesting that the disulfide bond involving this residue is indispensable for the responsiveness as has been reported by Clyne et al. (2002). The alanine-substitution of Pro²²⁵ also resulted in the loss of the ATP responsiveness (Fig. 2A). Proline residues are able to disturb the formation of rigid structures such as α -helixes or β -sheets. This ability of Pro²²⁵ may provide distortion necessary for Cys²²⁴ to contribute to the formation of the disulfide bond.

As for the substitutions of Ile²²⁶, the current response to ATP largely remained when substituted with valine (Fig. 2B,C). In contrast, the substitution with leucine resulted in a marked decrease in the current response (Fig. 2B,C). These results are puzzling because, among hydrophobic residues, leucine is similar to isoleucine in size but valine is smaller than these residues (Chothia, 1975). Interestingly, five of seven P2X receptor subclasses possess an isoleucine residue in this position, and the remaining two subclasses possess a valine residue (Fig. 1). Some common property between isoleucine and valine is necessary to maintain structures proper for the channel activation.

The substitutions of Phe²²⁷ with hydrophobic amino acid residues (leucine and isoleucine) resulted in the loss of the ATP responsiveness (Fig. 2A). Among P2X receptor subclasses, P2X₃ alone has leucine and all the remaining six subclasses have phenylalanine in this position. When Phe²²⁷ is replaced with leucine, five sequential amino acid residues beginning from Cys²²⁴ in P2X₂ receptor (cysteine–proline–isoleucine–leucine–arginine) completely accord with the

residues at corresponding positions in P2X₃ receptors (Fig. 1). In spite of this fact, the replacement resulted in the loss of the channel function.

The results obtained from the alanine-substitution of Arg²²⁸, Leu²²⁹ and Gly²³⁰ showed that a distinct reduction in the ATP responsiveness was found for L229A, but not for R228A or G230A (Fig. 3C). By combining these results and the results obtained from the substitutions of Ile²²⁶ and Phe²²⁷, it appears that the replacement of the residues at odd number positions more dramatically reduces the ATP responsiveness than that at even number positions (Fig. 5). Freist et al. (1998) have pointed out that a sequence stretch of the positions 170–330 in the extracellular loop of P2X receptor proteins exhibits similarities with the catalytic domains of class II aminoacyl-tRNA synthetases as shown by secondary structure predictions and sequence alignments. In their prediction, the region involving the above-mentioned amino acid residues participates in the formation of β -sheets. If these residues are involved in the β -sheets, the residues aligning in one side (Phe²²⁷ and Leu²²⁹) may be more influential on the channel function of P2X receptor than those in the other side (Ile²²⁶, Arg²²⁸ and Gly²³⁰).

The Hill coefficient of the wild-type P2X₂ receptor was about 2 (Fig. 4), which is in common with those in other reports (e.g., Nakazawa et al., 1991; Nakazawa, 1994). The value of 2 may indicate that the channel activation requires two ATP molecules (Tallarida and Jacob, 1979) though Bean (1990) has shown that the activation requires three ATP molecules at lower concentrations. The Hill coefficient of about 2 was not affected by the substitutions of the amino acid residues tested except for the alanine-substitution of Gly²³⁰ (Fig. 4). G230A exhibited a Hill coefficient of 1.3 when assuming homogenous binding sites (Fig. 4D, solid curve), but a better fitting could be obtained when the second binding sites of a lower affinity (Fig. 4D, broken curve). For the latter fitting, a Hill coefficient of about 2 was adopted for both the higher and the lower affinity sites. Thus, the introduction of alanine into the position 230 may not affect the number of ATP molecules for the channel activation, but may affect some process involved in the channel activation.

The present study and our previous studies (Nakazawa and Ohno, 1999; Nakazawa et al., 2002) have shown that small changes in a sequence from about the position 220 to about the position 260 in the extracellular loop can result in the loss of the ATP responsiveness. Jiang et al. (2000) also reported that alanine-substitution of Asn²⁰² or Asp²⁶¹ resulted in the loss of the ATP responsiveness. In addition, Buell et al. (1996) reported that P2X₄ receptor, which is insensitive to two-subclass selective purinoceptor antagonists (pyridoxal-5-phosphate-6-azophenyl-2',4'-disulfonic acid and pyridoxal 5-phosphate), restored sensitivities to these antagonists when Glu²⁴⁹ was replaced with lysine. These results suggest that this extracellular amino acid sequence may directly contribute to some indispensable process between the recognition of ATP molecules and the

channel opening. Ennion et al. (2000) suggested that basic amino acid residues close to the channel pore (Lys⁶⁸, Lys⁷⁰, Arg²⁹² and Arg³⁰⁹) serve to recognize ATP molecules in P2X₁ receptor and, thus, the ATP binding pocket may form close to the outer mouth of the channel pore. Similar results were also obtained for P2X₂ receptor (Jiang et al., 2000). The extracellular amino acid sequence described above (the positions 224–230) is not located between this possible binding pocket and the channel pore. If this sequence contributes to some indispensable process between the recognition of ATP molecules and the channel opening, it is desired that the sequence is spatially positioned close to the “activation” link between the binding pocket and the channel pore. This view may be supported by the slower activation process observed in the low responsiveness mutants (Fig. 6). It is possible that the extracellular loop is “packed” densely enough for the sequence to reach the “activation” link.

Acknowledgements

This work was partly supported by Health and Labour Science Research Grants for Research on Advanced Medical Technology from the Ministry of Health, Labour and Welfare, Japan, and a grant-in-aid for scientific research from the Ministry of Education, Science, Sports and Culture, Japan (KAKENHI 13672319) awarded to K.N.

References

- Bean, B.P., 1990. ATP-activated channels in rat and bullfrog sensory neurons: concentration dependence and kinetics. *J. Neurosci.* 10, 1–10.
- Brake, A.J., Wagenbach, M.J., Julius, D., 1994. New structural motif for ligand-gated ion channels defined by an ionotropic ATP receptor. *Nature* 371, 519–523.
- Buell, G., Lewis, C., Collo, G., North, R.A., Surprenant, A., 1996. An antagonist-insensitive P2X receptor expressed in epithelia and brain. *EMBO J.* 15, 55–62.
- Chothia, C., 1975. Structural invariants in protein folding. *Nature* 254, 304–308.
- Clyne, J.D., Wang, L.-F., Hume, R.I., 2002. Mutational analysis of the conserved cysteines of the rat P2X₂ purinoceptor. *J. Neurosci.* 22, 3873–3880.
- Ennion, S.J., Evans, R.J., 2002. Conserved cysteine residues in the extracellular loop of the human P2X₁ receptor form disulfide bonds and are involved in receptor trafficking to the cell surface. *Mol. Pharmacol.* 61, 303–311.
- Ennion, S., Hagan, S., Evans, R.J., 2000. The role of positively charged amino acids in ATP recognition by human P2X₁ receptors. *J. Biol. Chem.* 275, 29361–29367.
- Freist, W., Verhey, J.F., Stühmer, W., Gauss, D.H., 1998. ATP binding site of P2X channel proteins: structural similarities with class II aminoacyl-tRNA synthetases. *FEBS Lett.* 434, 61–65.
- Jiang, L.H., Rassendren, F., Surprenant, A., North, R.A., 2000. Identification of amino acid residues contributing to the ATP-binding site of a purinergic P2X receptor. *J. Biol. Chem.* 275, 34190–34196.
- Khakh, B.S., 2001. Molecular physiology of P2X receptors and ATP signalling at synapses. *Nat. Rev.* 2, 165–174.
- Nakazawa, K., 1994. ATP-activated current and its interaction with acetylcholine-activated current in rat sympathetic neurons. *J. Neurosci.* 14, 740–750.
- Nakazawa, K., Ohno, Y., 1999. Neighboring glycine residues are essential for P2X₂ receptor/channel function. *Eur. J. Pharmacol.* 370, R5–R6.
- Nakazawa, K., Fujimori, K., Takanaka, A., Inoue, K., 1991. Comparison of adenosine triphosphate- and nicotine-activated inward currents in rat phaeochromocytoma cells. *J. Physiol.* 434, 647–660.
- Nakazawa, K., Ohno, Y., Inoue, K., 1998. An aspartic acid residue near the second transmembrane segment of ATP receptor/channel regulates agonist sensitivity. *Biochem. Biophys. Res. Commun.* 244, 599–603.
- Nakazawa, K., Ojima, H., Ohno, Y., 2002. A highly conserved tryptophan residue indispensable for cloned rat neuronal P2X receptor activation. *Neurosci. Lett.* 324, 141–144.
- Newbolt, A., Stoop, R., Virginio, C., Surprenant, A., North, R.A., Buell, G., Rassendren, F., 1998. Membrane topology of an ATP-gated ion channel (P2X receptor). *J. Biol. Chem.* 273, 15177–15182.
- North, R.A., 2002. Molecular physiology of P2X receptors. *Physiol. Rev.* 82, 1013–1067.
- Soto, F., Garcia-Guzman, M., Stühmer, W., 1997. Cloned ligand-gated channels activated by extracellular ATP (P2X receptors). *J. Membr. Biol.* 160, 91–100.
- Tallarida, R.J., Jacob, L.S., 1979. *The Dose–Response Relation in Pharmacology*. Springer-Verlag, New York, NY.

Novel mechanism of tumorigenesis: Increased transforming growth factor- β 1 suppresses the expression of connexin 43 in BALB/cJ mice after implantation of poly-L-lactic acid

Saifuddin Ahmed, Toshie Tsuchiya

Division of Medical Devices, National Institute of Health Sciences, 1-18-1, Kamiyoga, Setagaya ku, Tokyo 158-8501, Japan

Received 15 December 2003; revised 24 March 2004; accepted 6 April 2004

Published online 4 June 2004 in Wiley InterScience (www.interscience.wiley.com). DOI: 10.1002/jbm.a.30090

Abstract: Poly-L-lactic acid (PLLA) is a widely used promising material for surgical implants such as tissue-engineered scaffolds. In this study, we aimed to determine the *in vivo* effect of PLLA plates on the cellular function of subcutaneous tissue in the two mouse strains, BALB/cJ and SJL/J, higher and lower tumorigenic strains, respectively. Gap-junctional intercellular communication (GJIC) and the expression of connexin 43 (Cx43) protein were significantly suppressed, whereas the secretion of transforming growth factor- β 1 (TGF- β 1) level was significantly increased in PLLA-implanted BALB/cJ mice compared with BALB/cJ controls. However, no significant difference in TGF- β 1 secretion was observed between the SJL/J-implanted and

SJL/J control mice. We found for the first time that a significant difference was observed between the two strains; thus, the PLLA increased the secretion of TGF- β 1 and suppressed the mRNA expression of Cx43 at the earlier stage after implantation into the higher-tumorigenic strain, BALB/cJ mice. This novel mechanism might have a vital role in the inhibition of GJIC and promote the tumorigenesis in BALB/cJ mice. © 2004 Wiley Periodicals, Inc. *J Biomed Mater Res 70A*: 335–340, 2004

Key words: poly-L-lactic acid; gap-junctional intercellular communication (GJIC); connexin 43; transforming growth factor (TGF)- β ; tumorigenesis

INTRODUCTION

The implantation of a biomaterial always induces a host inflammatory response. The extent and resolution of these responses have a vital role in determining the long-term success of implanted medical devices.^{1–3} Poly-L-lactic acid (PLLA) is a widely used material for surgical implants and clinically as a bioabsorbable suture material.^{4,5} Polyurethanes (PUs) have also been used for implant applications because of their useful elastomeric properties and high tensile strength, lubricity, and good abrasion resistance. Some adverse effects of the biomaterials, such as PLLA and PUs, have been reported in animal experiments. Long-term implants of PLLA produced tumorigenicity in rats.⁶

Correspondence to: T. Tsuchiya; e-mail: tsuchiya@nihs.go.jp
Contract grant sponsor: Health and Labour Sciences Research Grants

Contract grant sponsor: Research on Advanced Medical Technology, Ministry of Health, Labour and Welfare

Contract grant sponsor: Japan Health Sciences Foundation

© 2004 Wiley Periodicals, Inc.

Different kinds of PUs induced various tumor incidences in rats.⁷ All tumors have been generally viewed as the outcome of disruption of the homeostatic regulation of the cellular ability to respond to extracellular signals, which trigger intracellular signal transduction abnormalities.⁸ During the evolutionary transition from the single-cell organism to the multicellular organism, many genes appeared to accompany these cellular functions. One of these genes was the gene coding for a membrane-associated protein channel (the gap junction).⁹ Gap-junctional intercellular communications (GJIC) are transmembrane channels that allow the cell–cell transfer of small molecules and are composed of protein subunits known as connexin; at least 19 connexins exist and they are expressed in a cell- and development-specific manner.^{10,11} GJIC also has an important role in the maintenance of cell homeostasis and in the control of cell growth.¹² So, the loss of GJIC has been considered to cause abnormal development and tumor formation.^{13–15} Several tumor promoters have been shown to restrict GJIC by phosphorylation of connexin proteins, such as connexin 43 (Cx43), which is an essential

protein to form the gap-junction channel.^{16,17} We have hypothesized that the different tumorigenic potentials of PLLA and PUs are caused mainly by the different tumor-promoting activities of these biomaterials. Therefore, we investigated the effects of PLLA on the subcutaneous tissue between the two strains of female mice, BALB/cJ and SJL/J.

MATERIALS AND METHODS

Animals

Five-week-old female BALB/cJ and SJL/J mice were purchased from Charles River (Japan) and maintained in the animal center according to the animal welfare National Institute of Health Sciences guidance. All mice were fed with standard pellet diets and water *ad libitum*, before and after the implantation.

Implantation of PLLA

PLLA was obtained from Shimadzu Co. Ltd. as uniform plates. Implants (size: 20 × 10 × 1 mm, weight-average molecular weight 200,000) were sterilized using ethylene oxide gas before use. Sodium pentobarbital (4 mg/kg) was intraperitoneally administered to the mice. The dorsal skin was shaved and scrubbed with 70% alcohol. Using an aseptic technique, an incision of approximately 2 cm was made; away from the incision, a subcutaneous pocket was formed by blunt dissection, and one piece of PLLA was placed in the pocket. The incision was closed with silk threads. In both strains, controls were obtained by sham operation and subsequent subcutaneous pocket formation. After surgery, the mice were housed in individual cages. After 30 days, mice from the implanted group were sacrificed, implanted materials were excised out, and subcutaneous tissues from the adjacent sites were collected for culture. At the same time, subcutaneous tissues were removed from the sites in the sham-operated controls that correlated with the implant sites.

Cell culture of subcutaneous tissues

The subcutaneous tissues were maintained in minimum essential medium supplemented with 10% fetal bovine serum in a 5% CO₂ atmosphere at 37°C.

Scrape-loading and dye transfer (SLDT) assay

SLDT technique was performed by the method of El-Fouly et al.¹⁸ Confluent monolayer cells in 35-mm culture dishes were used. After rinsing with Ca²⁺ Mg²⁺ phosphate-

buffered saline [PBS (+)], cell dishes were loaded with 0.1% Lucifer Yellow (Molecular Probes, Eugene, OR) in PBS (+) solution and were scraped immediately with a sharp blade. After incubation for 5 min at 37°C, cells were washed three times with PBS (+) and the extent of dye transfer was monitored using a fluorescence microscope, equipped with a type UFX-DXII CCD camera and super high-pressure mercury lamp power supply (Nikon, Tokyo, Japan).

Western blot analysis

When cells grew confluent in 60-mm tissue culture dishes, all cells were lysed directly in 100 μL of 2% sodium dodecyl sulfate (SDS) gel loading buffer (50 mM Tris-HCl, pH 6.8, 100 mM 2-mercaptoethanol, 2% SDS, 0.1% bromophenol blue, 10% glycerol). The protein concentration of the cleared lysate was measured using the microplate BCA (bicinchoninic acid) protein assay (Pierce, Rockford, IL). Equivalent protein samples were analyzed by 7.5% SDS-polyacrylamide gel electrophoresis. The proteins were transferred to Hybond-ECL nitrocellulose membranes (Amersham Pharmacia Biotech UK Ltd., Buckinghamshire, UK). Cx43 protein was detected by anti-Cx43 polyclonal antibodies (ZYMED Laboratories, Inc., San Francisco, CA). The membrane was soaked with Block Ace (Yukijirusi Nyugyo, Sapporo, Japan), reacted with the anti-Cx43 polyclonal antibodies for 1 h, and after washes with PBS containing 0.1% Tween20, reacted with the secondary anti-rabbit immunoglobulin G antibody conjugated with horseradish peroxidase for 1 h. After several washes with PBS-Tween20, the membrane was detected with the ECL detection system (Amersham Pharmacia Biotech UK Ltd.).

Reverse transcriptase polymerase chain reaction (RT-PCR)

Cx43 mRNA expression was verified by RT-PCR. Total cellular RNA was isolated from cultured cells in Trizol reagent (Life Technologies, Inc., Frederick, MD) following the manufacturer's instructions. The concentration of total RNA was determined using a UV spectrophotometer (Gene Quant; Pharmacia Biotech, Piscataway, NJ). cDNA was synthesized from 1 μg of total RNA by RT using the First-Strand cDNA synthesis kit (Amersham Pharmacia Biotech, Uppsala, Sweden). Amplification was performed in a volume of 25 μL containing 1 μL of cDNA, 10 pmol of each primer, 0.625 unit of *Taq* polymerase (Promega, Madison, WI) and 0.2 mM of each deoxynucleotide triphosphate. The sequence of the primer pairs were as follows: forward 5'-ACAGTCTGCCTTCGCTGTAAC-3' and reverse 5'-GTAAGGATCGCTTCTCCCTTC-3'. The PCR cycle was as follows: initial denaturation at 94°C for 5 min, followed by 25 cycles of 94°C for 1 min, 60°C for 1 min, and 72°C for 1 min, with final extension at 72°C for 7 min. The amplified product was separated on 1.5% agarose gel and visualized with SYBR Green I (BioWhittaker Molecular Applications, Rockland, ME). For relative quantitation, the signal intensity of each lane was standardized to that of a housekeeping gene,

GAPDH. To amplify this gene, the following primer pairs were used: forward 5'-CCCATCACCATCTCCAGGAGC-GAGA-3' and reverse 5'-TGGCCAAGGTCATCCATGACAACTTTGG-3'.

Enzyme-linked immunosorbent assay (ELISA)

Cells were seeded onto 60-mm dishes. The conditioned medium was collected and obtained after the centrifugation at 1000 rpm for 2 min. The transforming growth factor (TGF)- β levels of the media were measured with commercially available ELISA kits (R&D Systems Inc., Minneapolis, MN).

Cytokine treatment

Here, we used sham-operated BALB/cj mice cells as a control. One hundred thousand cells were seeded onto 35-mm tissue culture dishes and cultured. After 4 h seeding in a 5% CO₂ atmosphere at 37°C, cells were treated with TGF- β 1 (0, 2, and 10 ng/mL). Thereafter, SLDT and RT-PCR were performed. Purified human TGF- β 1 was purchased from R&D Systems.

Statistical analysis

Student *t* test was used to compare the implanted samples with the controls. Statistical significance was accepted at *p* < 0.05. Values were presented as the mean \pm standard deviation.

RESULTS AND DISCUSSION

There are many known tumorigenesis-inducing factors. It was reported that many plastics induce malignant tumors when implanted subcutaneously into rats and mice.¹⁹⁻²² PLLA shows slow degradation, and therefore has been applied as a biomaterial for surgical devices such as bone plates, pins, and screws. It was reported in different studies that polyetherurethane, polyethylene, and PLLA produced tumors in rats.^{6,7,23-25} In our study, tumors were induced by PLLA plates in BALB/cj mice at 100% incidence but not in SJL/J mice at the surrounding tissues of PLLA plates during a 10-month *in vivo* study. To understand the mechanisms of tumorigenesis induced by PLLA, we focused on the inhibitory effects on GJIC at the early stage of tumorigenesis. To assess functional GJIC, the SLDT assay was performed. Brand et al.²⁶ reported that BALB/cj mice are a higher and SJL/J mice are a lower tumorigenic strain. Our present re-

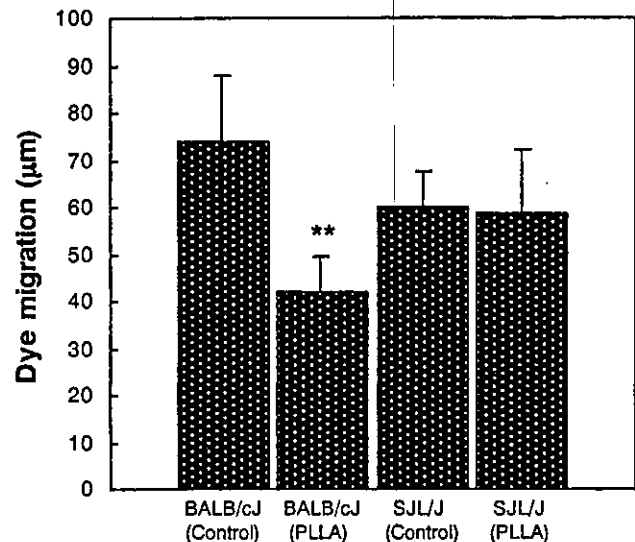


Figure 1. Statistical analysis of the SLDT assay. In both the implanted and sham-operated controls, three mice of each strain were sacrificed after 30 days. Results shown are representative of two independent experiments. GJIC was significantly inhibited in PLLA-implanted BALB/cj mice cells compared with BALB/cj controls. ***p* < 0.01.

sults showed that the GJIC was significantly inhibited in 1-month PLLA-implanted BALB/cj mice cells compared with BALB/cj controls (Fig. 1). In contrast, no significant difference was observed between the 1-month PLLA-implanted SJL/J mice and SJL/J controls (Fig. 1). The data also revealed that the dye migration was higher in control BALB/cj mice than control SJL/J mice (Fig. 1). High responder to the tumorigenicity may be classified as animals that are easily suppressed in both GJIC function and the connexins expression. This perturbed gap junction is likely to have a major role in the PLLA-induced tumorigenesis. Gap junctions are also regulated by the posttranslational phosphorylation of the carboxy-terminal tail region on the connexin molecule. Phosphorylation of connexin molecules is closely related with the inhibition of GJIC.^{27,28} Phosphorylation has been involved in controlling a broad variety of connexin processes that include trafficking, gathering/nongathering, degradation, and also the gating of gap channels. It was also reported that communication-deficient cells did not express the Cx43-biphosphorylated (P₂) isoform but cells with low gap-junction permeability showed detectable amounts of the Cx43-monophosphorylated (P₁) isoform.¹⁶ To survey the cause, we examined the mRNA and protein expression of the Cx43 gene. Here, mRNA expression was suppressed in PLLA-implanted BALB/cj mice compared with BALB/cj controls [Fig. 2(A)]. No significant difference was observed between the PLLA-implanted SJL/J mice and SJL/J controls [Fig. 2(B)]. We also found that the total level of protein expression such as unphos-

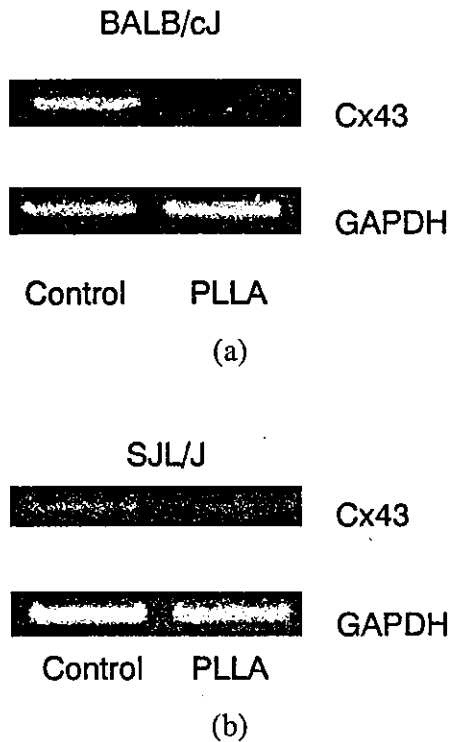


Figure 2. mRNA expression of Cx43 by RT-PCR analysis. In both the implanted and sham-operated controls, three mice of each strain were sacrificed after 30 days. Results shown are representative of two independent experiments. SYBR Green I stained PCR products after agarose gel electrophoresis showed that (A) mRNA expression was suppressed in PLLA-implanted BALB/cJ mice compared with BALB/cJ controls, and (B) no significant difference was observed between the PLLA-implanted SJL/J mice and SJL/J controls.

phorylated (P_0), P_1 , and P_2 levels were significantly decreased in PLLA-implanted BALB/cJ mice compared with the control (Fig. 3). Asamoto et al.²⁹ reported that tumorigenicity was enhanced when the expression of Cx43 protein was suppressed by the anti-sense RNA of Cx43. A similar tendency was also observed in our study where the protein expression might be inhibited via down-regulation of the mRNA level. The genetic alteration and posttranslational

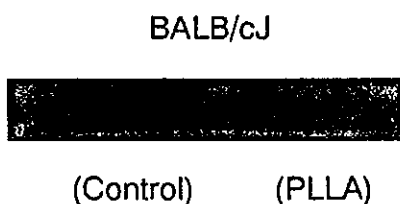


Figure 3. Protein expression of Cx43 by Western blot analysis. In both the implanted and sham-operated controls, three mice of each strain were sacrificed after 30 days. Results shown are representative of two independent experiments. Total level of protein expression such P_0 , P_1 , and P_2 levels were significantly decreased in PLLA-implanted BALB/cJ mice compared with the controls.

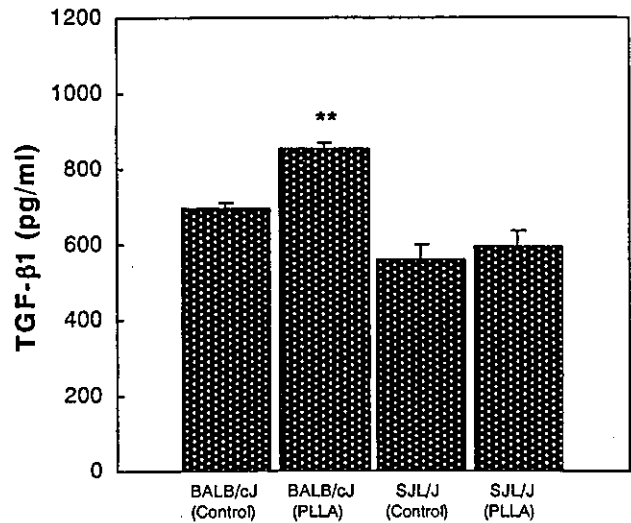


Figure 4. Statistical analysis of TGF-β1 cytokine assay by ELISA. In both the implanted and sham-operated controls, three mice of each strain were sacrificed after 30 days. Results shown are representative of two independent experiments. Secretion of the TGF-β1 level was significantly increased in PLLA-implanted BALB/cJ mice compared with BALB/cJ controls. ** $p < 0.01$.

modification in the Cx43 protein was shown to be involved in impaired GJIC and could be associated with tumorigenesis. Therefore, it is suggested that the inhibitory effect of PLLA on GJIC might be caused by the alteration in the Cx43 protein, causing enhancement of tumorigenesis. Moreover, Moorby and Patel³⁰ reported a direct action of the Cx43 protein on cell growth that was mediated via the cytoplasmic carboxyl domain.

Because TGF-β1 inhibits GJIC by decreasing the phosphorylated form of Cx43³¹ and the phosphorylation of Cx43 has been implicated in gap-junction assembly and gating events,^{16,27,32} we hypothesized that TGF-β1 might have an important role on PLLA-implanted BALB/cJ mice. Figure 4 clearly demonstrates that the secretion of the TGF-β1 level was significantly increased in PLLA-implanted BALB/cJ subcutaneous tissue in comparison with those from BALB/cJ control mice. No significant difference was found in the secretion of TGF-β1 between the SJL/J implanted and SJL/J control mice. TGF-β2 and TGF-β3 cytokine assay revealed no significant difference in TGF-β2 secretion and TGF-β3 was below the detection level (data not shown). So we performed an *in vitro* study, which showed that the intercellular communication and the mRNA expression of Cx43 were significantly suppressed in BALB/cJ control cells when treated with TGF-β1 [Fig. 5(A,B)].

In conclusion, we suggest that increased secretion of TGF-β1 (Fig. 4) suppressed expression of the gap-junctional protein Cx43 (Fig. 3) at the earlier stage after implantation of PLLA in BALB/cJ mice, resulting in